

Identification of functional lipid metabolism biomarkers of brown adipose tissue aging



Sabrina Gohlke¹, Vyacheslav Zagoriy², Alvaro Cuadros Inostroza², Michaël Méret², Carola Mancini¹, Lukasz Japtok³, Fabian Schumacher^{3,4}, Doreen Kuhlow¹, Antonia Graja¹, Heike Stephanowitz⁵, Markus Jähnert^{6,7}, Eberhard Krause⁵, Andreas Wernitz⁸, Klaus-Jürgen Petzke⁸, Annette Schürmann^{6,7}, Burkhard Kleuser^{3,9}, Tim J. Schulz^{1,7,10,*}

ABSTRACT

Objective: Aging is accompanied by loss of brown adipocytes and a decline in their thermogenic potential, which may exacerbate the development of adiposity and other metabolic disorders. Presently, only limited evidence exists describing the molecular alterations leading to impaired brown adipogenesis with aging and the contribution of these processes to changes of systemic energy metabolism.

Methods: Samples of young and aged murine brown and white adipose tissue were used to compare age-related changes of brown adipogenic gene expression and thermogenesis-related lipid mobilization. To identify potential markers of brown adipose tissue aging, non-targeted proteomic and metabolomic as well as targeted lipid analyses were conducted on young and aged tissue samples. Subsequently, the effects of several candidate lipid classes on brown adipocyte function were examined.

Results: Corroborating previous reports of reduced expression of uncoupling protein-1, we observe impaired signaling required for lipid mobilization in aged brown fat after adrenergic stimulation. Omics analyses additionally confirm the age-related impairment of lipid homeostasis and reveal the accumulation of specific lipid classes, including certain sphingolipids, ceramides, and dolichols in aged brown fat. While ceramides as well as enzymes of dolichol metabolism inhibit brown adipogenesis, inhibition of sphingosine 1-phosphate receptor 2 induces brown adipocyte differentiation.

Conclusions: Our functional analyses show that changes in specific lipid species, as observed during aging, may contribute to reduced thermogenic potential. They thus uncover potential biomarkers of aging as well as molecular mechanisms that could contribute to the degradation of brown adipocytes, thereby providing potential treatment strategies of age-related metabolic conditions.

© 2019 The Authors. Published by Elsevier GmbH. This is an open access article under the CC BY-NC-ND license (<http://creativecommons.org/licenses/by-nc-nd/4.0/>).

Keywords Brown adipose tissue; Aging; Ceramides; Sphingolipids; Dolichol lipids

1. INTRODUCTION

Adipose tissue is a metabolically active organ that plays a central role in the regulation of systemic energy balance and the development of metabolic diseases, including obesity and type-2 diabetes mellitus. While the main function of white adipose tissue (WAT) is the storage of energy in the form of triacylglycerols, the specialized brown adipose tissue (BAT) utilizes nutrients to produce heat, a process known as non-shivering or adaptive thermogenesis [1,2]. This process is made possible by the activity of the uncoupling protein 1 (UCP1) which is exclusively expressed in brown adipocytes. Located in the inner mitochondrial membrane, it uncouples the mitochondrial proton gradient from ATP production. Activation of UCP1 and mitochondrial thermogenesis depend on the β 3-adrenergic receptor which is activated by noradrenaline released by sympathetic neurons in response to

cold. It is well-established that BAT is present and metabolically active in adult humans and localizes mainly to the neck and upper body regions [3–5]. A second type of UCP1-expressing adipocytes, the beige or brite (brown-in-white) adipocytes, occur in WAT depots and are recruited upon prolonged cold exposure or direct adrenergic stimulation, in a process known as browning [6,7].

Aging is a negative regulator of brown adipocyte formation and function. In humans, loss of BAT mass is observed with increasing age and is accompanied by attenuated activation of thermogenesis [5]. Similar findings have also been reported in rodent models [8]. This loss of thermogenic capacity may be due to a phenotypic switch described as whitening, e.g. the conversion of brown into white-like adipose tissue, which is accompanied by reduced UCP1 expression and activity [8]. The thermogenic defect has also been linked to mitochondrial dysfunction of mature brown adipocytes and reduced proliferative

¹Department of Adipocyte Development and Nutrition, German Institute of Human Nutrition Potsdam-Rehbrücke, Nuthetal, Germany ²metaSysX GmbH Potsdam Golm, Germany ³Department of Toxicology, Institute of Nutritional Science, University of Potsdam, Potsdam-Rehbrücke, Nuthetal, Germany ⁴Department of Molecular Biology, University of Duisburg-Essen, Essen, Germany ⁵Leibniz Institute for Molecular Pharmacology, Berlin, Germany ⁶Department of Experimental Diabetology, German Institute of Human Nutrition Potsdam-Rehbrücke, Nuthetal, Germany ⁷German Center for Diabetes Research (DZD), München, Neuherberg, Germany ⁸Department of Molecular Epidemiology, German Institute of Human Nutrition Potsdam-Rehbrücke, Nuthetal, Germany ⁹NutriAct – Competence Cluster Nutrition Research, Berlin, Potsdam, Germany ¹⁰Institute of Nutritional Science, University of Potsdam, Potsdam-Rehbrücke, Nuthetal, Germany

*Corresponding author. German Institute of Human Nutrition, Potsdam-Nuthetal, D-14558, Germany. E-mail: tim.schulz@dife.de (T.J. Schulz).

Received December 10, 2018 • Revision received March 22, 2019 • Accepted March 28, 2019 • Available online 4 April 2019

<https://doi.org/10.1016/j.molmet.2019.03.011>

expansion of brown adipogenic progenitor cells [9]. Further, brown adipose tissue may lose the ability to respond to adrenergic stimulation due to a defect in post-receptor signaling events [10]. Brown and white adipose tissues are endocrine organs that secrete a range of hormones and metabolites, thereby regulating metabolic homeostasis. Several lines of evidence suggest that secreted products of adipose tissue lipid metabolism, the lipokines, may contribute essential regulatory cues to integrate nutrient handling in adipose tissues and other organs, thereby affecting systemic lipid homeostasis as well as the development of metabolic dysfunction [11,12]. For instance, cardiolipins in BAT were recently described as important regulators of energy metabolism [13,14], and the thermogenic lipokine, 12,13-diHOME, is involved in the activation of BAT in response to cold, leading to an increase of fatty acid uptake [15]. This is important since excess serum fatty acids (FA) may trigger inflammatory responses by activating toll-like receptors (TLRs) which could lead to insulin resistance [16]. In dysfunctional adipose tissue, an increased appearance of lipotoxic intermediates, such as ceramides and diacylglycerols (DAG), has been observed [17]. DAGs can activate certain protein kinase C (PKC) isoforms which inhibit insulin signaling in liver and muscle [18]. Additionally, fatty acids are precursors for the biosynthesis of ceramides, which have been linked to oxidative stress, lipotoxicity and inhibition of insulin signaling [19]. Prevention of ceramide production by inhibition of ceramide synthases in turn promotes the browning of WAT and improves glucose and lipid metabolism [20]. In summary, the effects of various lipid species on adipose tissue could play a central role in the emergence of metabolic pathologies, such as adiposity, dyslipidemia, and insulin resistance. However, very little is known about age-related changes of lipid metabolites in BAT, their involvement in BAT-dysfunction and the contribution of this process to metabolic disorders. To identify functional lipid biomarkers of brown adipose tissue aging, we combined metabolomic and proteomic analyses to compare BAT and WAT from mice collected at different ages. These correlational analyses reveal that changes of several lipid classes and individual metabolite species correlate with adipose tissue aging. Among these, sphingolipids are significantly induced in aged BAT. Uncovering a potential function of this lipid class in age-related BAT-dysfunction, we show that ceramides and activation of sphingosine 1-phosphate signaling inhibit the thermogenic potential of brown adipocytes. Dolichols, a group of prenolic lipid-derivatives that function as substrates for the enzyme dolichol kinase, are increased in aged BAT and inguinal white adipose tissue (iWAT). Modulation of dolichol kinase expression inversely correlates with brown adipogenesis. Our findings show that age-related alterations of lipid metabolism may result in increased formation of bioactive lipid species in adipose tissues that exert detrimental effects on brown/beige adipocyte formation and thermogenic function.

2. EXPERIMENTAL PROCEDURES

2.1. Tissue collection

All procedures were approved by the ethics committee for animal welfare of the State Office of Environment, Health, and Consumer Protection (State of Brandenburg, Germany). Male C57Bl6J mice (Charles River Laboratories, Sulzfeld, Germany), *S1pr2*-deficient mice (B6.129-S1pr2tm1Jch) and *Dolk*-heterozygous mice (C57BL/6NJ-Dolkem1(IMPC)J/J, The Jackson Laboratory strain 026820) were housed in a controlled environment (22 ± 2 °C, 12/12 h light/dark cycle), maintained on a standard diet (Ssniff, Soest, Germany). For cold exposures, room temperature was reduced stepwise every other day until reaching 5 °C, the temperature at which animals were kept for an

additional three days before organ collection. To this end, the temperature was initially reduced by 7 °C from 22 °C to 15 °C for two days. After this the temperature was reduced by 5 °C every other day, from 15 °C to 10 °C and then from 10 °C to 5 °C. Animals were killed by cervical dislocation. AT depots were isolated, immediately frozen in liquid nitrogen, and stored at –80 °C until analysis. The tissues were ground while kept frozen in liquid nitrogen and powder was aliquoted for the different analyses.

2.2. Ex vivo lipolysis analysis in adipose tissue explants

Adipose tissue of dissected mice was cut into small pieces (weight approximately 10 mg) and subsequently washed in PBS. 3 × 3 pieces were transferred to a 96 well containing 150 µl of explant medium (DMEM without phenol red) containing 2% fatty acid free BSA (Sigma Aldrich, Taufkirchen, Germany) and supplemented either with 10 µM norepinephrine (Sigma Aldrich, Taufkirchen, Germany) or 10 µM isoproterenol (Sigma Aldrich, Taufkirchen, Germany) as indicated in the respective figures. After 2 h of incubation at 37 °C and 5% CO₂, conditioned medium was collected and centrifuged before storing at –80 °C for later analysis of glycerol release using a Cobas Mira analyzer (Roche, Basel, Switzerland). Explants were collected and subsequently homogenized in RIPA buffer (Sigma Aldrich, Taufkirchen, Germany) containing phosphatase and protease inhibitors (Sigma Aldrich, Taufkirchen, Germany) for total protein contents and protein expression analysis by immunoblotting.

2.3. FACS staining

AT-derived progenitor cells were isolated from the BAT and iWAT of mice according to published procedures [21,22]. In brief, cells stained positive for surface antigen Stem cell antigen 1 (Sca1, #17-5981-82, Thermo Fisher Scientific, Dreieich, Germany) and negative for the hematopoietic marker antigen CD45 (#11-0451-82, Thermo Fisher Scientific, Dreieich, Germany) and the endothelial marker antigen CD31 (#11-0311-82, Thermo Fisher Scientific, Dreieich, Germany) were purified by fluorescence-activated cell sorting (FACS, BD FACSAria™ III, BD Biosciences, San Jose, CA, USA). Cells were cultivated as described previously [22].

2.4. Adipogenic progenitor cell (APC) differentiation with sphingolipid exposure

Primary, FACS-isolated APCs were differentiated as described before with minor modifications [22]. In brief, after seeding cells were grown to confluence for three days with 1 µM rosiglitazone (Sigma Aldrich, Taufkirchen, Germany). Cell differentiation was induced with culture medium containing 2% fetal bovine serum, 0.8 µM human recombinant insulin, 50 µM indomethacin, 0.5 µM 3-Isobutyl-1-methylxanthin (IBMX), 1 µM dexamethasone and 1 nM thyroid hormone triiodothyronine (T3) for two days followed by 7 days of adipogenesis in differentiation media supplemented with insulin and T3 only. The brown adipogenic cell line WT1 [23] was seeded and differentiated after three days of proliferation. After two days of induction media containing 2% fetal bovine serum, 20 nM human recombinant insulin, 0.125 mM indomethacin, 0.5 mM IBMX, 5 µM dexamethasone and 1 nM T3, cells were differentiated from day 5 to day 10 in media with insulin and T3. Medium was refreshed every other day. Whenever indicated in the figures, differentiated cells were treated with 1 µM norepinephrine or 1 µM of isoproterenol for 4 h before harvest (both Sigma Aldrich, Taufkirchen, Germany). For sphingolipid experiments, cells were exposed to ceramide and sphingosine 1-phosphate (S1P) during the differentiation phase, as indicated in the figure legend. Ceramide C16 (d18:1/C16; Enzo Life sciences, Lörrach Germany) was dissolved in

ethanol as stock solution and added to a final concentration of 5–10 μM S1P (Tocris Bioscience, Wiesbaden-Norderstedt, Germany) was dissolved in phosphate-buffered saline as a complex with bovine serum albumin (4 mg/ml) as stock solution and used in concentrations ranging from 0.5 to 5 μM . Ceramide synthase inhibitor fumonisins B1 and S1P receptor antagonists JTE013 (JTE), CYM 50358 hydrochloride (CYM) and VPC23019 (VPC; all from Tocris Bioscience, Wiesbaden-Norderstedt, Germany) were dissolved in DMSO and used at final concentration ranges of 0.1–1 μM .

2.5. Quantitative real-time PCR

RNA was isolated from ground tissue powder by using a commercially available RNA MiniPrep Kit (Zymo Research, Freiburg, Germany). Purified RNA was transcribed into cDNA with a high capacity cDNA reverse transcription kit (Thermo Fisher Scientific, Dreieich, Germany). Quantitative real-time PCR quantification was conducted using Maxima SYBR Green/ROX qPCR Master Mix (Thermo Fisher Scientific, Dreieich, Germany) and the Real-Time PCR system CFX384 Touch (Bio-Rad, München, Germany) and using intron-spanning primers to specifically amplify cDNA (Table S9).

2.6. Immunoblotting

Samples were homogenized in RIPA buffer, and protein concentrations were determined with a BCA protein assay kit (Thermo Fisher Scientific, Dreieich, Germany). The protein samples were separated via SDS-polyacrylamide gel electrophoresis and transferred to PVDF membranes. Proteins were detected using the following antibodies: anti-UCP1-ab (Genetex, Irvine, CA, USA), anti-phospho-HSL-ab, anti-HSL-ab, anti-phospho(S9)-GSK3b-ab, anti-GSK3b-ab (all from Cell Signaling Technology, Danvers, MA, USA), anti-phospho(S293)-PDH-ab and anti-PDH-ab (all from Abcam, Cambridge, United Kingdom) or anti-DOLK-ab (Abcam, Cambridge, United Kingdom) followed by incubation with a horseradish-peroxidase-conjugated secondary antibody. As loading controls, HRP-conjugated anti- β -Actin-ab signals (Sigma Aldrich, Taufkirchen, Germany) were used.

2.7. Mitochondrial respiration

WT1 cells were seeded into XF96 cell culture plates (Agilent Technologies, Waldbronn, Germany) and grown to confluency. After ten days of differentiation as described under 2.4, oxygen consumption was measured on a Seahorse XF96 Flux Analyzer (Agilent Technologies, Waldbronn, Germany). In brief, all measurements were conducted in triplicates as cycles of 3 min mixing and 3 min measurement. Inhibition of mitochondrial respiration was measured after injection of 2 μM oligomycin (Tocris Bioscience Wiesbaden-Norderstedt, Germany). Addition of 1 μM Carbonyl-cyanide-4-(trifluoromethoxy)-phenylhydrazone (FCCP; Sigma, Taufkirchen, Germany) was used for measurement of maximal respiration capacity. Non-mitochondrial respiration was measured after injection of 0.5 μM each of rotenone and antimycin A (Sigma, Taufkirchen, Germany). After each addition, a similar measurement cycle was conducted. Oxygen consumption rate (OCR) was normalized to cell density as determined by staining cells with 4',6-Diamidino-2-Phenylindole, Dihydrochloride (DAPI, BioLegend, London, United Kingdom) and measurement of fluorescence on a SynergyH1 plate reader (BioTek, Bad Friedrichshall, Germany) at excitation/emission wavelengths of 358/461 nm after Seahorse measurements were completed.

2.8. Targeted lipid analysis

Ceramides were extracted from 10 mg of ground brown adipose tissue with ceramide C19 (Avanti Polar Lipids, Alabaster, Alabama, USA) as

internal standard using chloroform/methanol 1/2 (v/v). After addition of 1 M KOH, samples were neutralized with glacial acetic acid and the lower phase containing ceramides was re-extracted with chloroform. After drying, sample pellets were re-suspended in mobile phase A (1 mM ammoniumformiate in methanol with 0.2% formic acid) and measured on QTOF mass spectrometer LC-MS 6530 (Agilent Technologies, Waldbronn, Germany) in positive electrospray ionization mode (ESI+) on a C8 separation column. Ceramides were identified due to exact masses (m/z) and subsequent fragmentation of the target ion as described [24]. Intensities were normalized to internal standard C19 and normalized to samples' protein content.

2.9. Fatty acid (FA) analysis by gas chromatography

Analysis of FA spectra was performed with a previously published method that was modified as follows [25,26]: Brown and inguinal white adipose tissues were ground in liquid nitrogen and 10 mg of tissue powder was homogenized in phosphate buffered saline and protein concentrations were determined using a BCA protein assay kit (Thermo Fisher Scientific, Dreieich, Germany) for normalization of FA amount. Lipids were extracted with tert-butyl methyl ether containing 0.01% butyl hydroxytoluene/methanol solution (2/1, v/v). The lipid fraction was evaporated under N₂ and re-dissolved for bonded phase column separation (SPE) in chloroform. Firstly, neutral lipids and free FA were eluted with chloroform/methanol/acetic acid (100/2/2, v/v). After changing vials, the PL fraction was eluted with methanol. Solvents were evaporated under a stream of N₂ at 40 °C.

For hydrolysis and methylation of FA, the dried PLs were re-dissolved in toluene. Trimethyl sulfonium hydroxide solution (TMSH, Macherey–Nagel, Düren, Germany) was added to form FA methyl esters (FAME). Internal standard was added (C21:0, heneicosanoic acid) before TMSH reaction, FAME were analyzed by gas chromatography using an Agilent GC system 7890A equipped with Agilent 7000 GC/MS Triple Quad (Agilent Technologies, Waldbronn, Germany) and a flame ionization detector (FID). Samples were injected in split-less mode at 30 °C, 30–260 °C, ramp 12 °C/s, held 2 min, 260–320 °C, ramp 12 °C/s and separated on a GC capillary column (HP-88, 100 m \times 0.25 mm I.D., 0.2 μm film thickness, Agilent, Waldbronn, Germany) under constant Helium carrier gas flow. A gas chromatography oven temperature program was employed as follows: Start at 80 °C, held 1 min, 80–170 °C, ramp 10 °C/min, held 5 min, 170–175 °C, ramp 5 °C/min, 175–190 °C, ramp 2 °C/min, 190–205 °C, ramp 5 °C/min, 205–235 °C, ramp 5 °C/min, held 8 min, total run time 57.5 min. For identification and column check-out a 37-component FAME mixture (Supelco/Sigma Aldrich, Taufkirchen, Germany) was used.

2.10. HPLC analysis

Adipose tissue samples were ground in liquid nitrogen and subsequently transferred to glass tubes containing 2 ml of 5 M KOH solution. 3 ml methanol was added and the samples were incubated for 1 h at room temperature and 1 h at 100 °C in a water bath. After cooling, internal dolichol standards Dol C115 (Hartmann Analytic, Braunschweig, Germany) and Coenzyme Q6 (Avanti Polaris, Alabaster, Alabama, USA) were added. Lipids were then extracted with hexane (Sigma Aldrich, Taufkirchen, Germany). After washing the lipid-containing phase with water at least three times, the pure lipid containing hexane phase was evaporated under vacuum. Dolichols were re-suspended in 500 μl chloroform/methanol (2/1) and analyzed on a HPLC instrument (Dionex, Sunnyvale, California, USA) using a C18 reversed-phase Spherisorb ODS2-150 mm column (Waters Corporation, Milford, Massachusetts, USA) kept in a column oven (Dionex, Sunnyvale, California, USA) at a stable

temperature of 30 °C. The mobile phase was MeOH/isopropanol/H₂O (60/30/5). Dolichols were eluted with hexane/isopropanol (70/30) using a gradient from 20% to 70% phase B with increasing concentrations of phase B over 20 min. An ultraviolet detector (MWD-3000 UV detector Thermo Fisher Scientific, Dreieich, Germany) was used for detection of dolichols at 214 nm. Dolichols were identified due to retention times compared to standard mixtures (Avanti Polar Lipids, Alabaster, Alabama, USA) and separated because of increasing numbers of carbon atoms in their backbone. Peak intensity was normalized first to internal standard Dolichol C115 and second to total protein content in adipose tissue lysate measured with BCA assay kit (Thermo Fisher Scientific, Dreieich, Germany).

2.11. Comparative proteomic analysis

Two independent comparisons of young and old tissue samples were performed. Specifically, tissue extracts of BAT collected from five age-matched mice were pooled to generate each sample. Each sample pair was measured in duplicate, where either the young or the old sample of each pool were labeled with ¹⁸O prior to analysis. Proteins were separated by 12% polyacrylamide gel electrophoresis. Equally sized pieces of Coomassie stained protein bands were excised from all lanes of the gel, covering the entire length of each lane. Protein digestion and in-gel ¹⁶O/¹⁸O-labeling was performed as described [27]. In brief, the gel pieces were incubated with 50 ng trypsin (sequencing grade modified, Promega; Madison, Wisconsin, USA) in 10 µL of 50 mM ammonium bicarbonate. The tryptic digestions were performed in the presence of ¹⁸O-labeled water (Campro Scientific GmbH, 97% ¹⁸O; Berlin, Germany) and normal water for young and old tissue samples, respectively. 10 µL of 0.5% TFA in acetonitrile was added and the separated supernatant was dried under vacuum. Samples were reconstituted in 3 µL of 0.1% (v/v) TFA, 5% (v/v) acetonitrile in water and paired gel slices (160 and 180 samples of adjoining slices) were combined immediately before nano-LC-mass spectrometry analysis. Mass spectrometric analysis was performed using Nano-LC-ESI-MS/MS (Orbitrap Elite, Thermo Fisher Scientific; Schwerte, Germany). The processed MS/MS spectra and MASCOT server (version 2.2, Matrix Science Ltd., London) were used to search in-house against the UniProtKB/Swiss-Prot database MOUSE 2013okt (51193 sequences; 24573350 residues). The maximum of two missed cleavages was allowed and the mass tolerance of precursor and sequence ions was set to 10 ppm and 0.35 Da, respectively. Acrylamide modification of cysteine, methionine oxidation, and C-terminal 1801- and 1802-isotope labeling were considered as possible modifications. A protein was accepted as unambiguously identified if the total MASCOT score was greater than the significance threshold and if at least 2 peptides appeared the first time in the report and were the top ranking peptides. Based on decoy database searches, the false positive rate was estimated to be <1%. Quantification was carried out using the Mascot Distiller Quantitation Toolbox (version 2.2.1.2, Matrix Science Ltd., London; Great Britain) and was based on calculations of isotope intensity ratios of at least two tryptic peptides with individual MASCOT scores indicating at least homology. Relative protein ratios (H/L) were calculated from the intensity-weighted average of all peptide ratios. Pathway clustering for proteins either reduced (H/L ratio < 1) or enriched (H/L ratio > 2.5) in aged BAT samples were annotated to appropriate pathways based on KEGG classification using Enrichr web server [28,29]. Gene ontology (GO) terms were annotated to proteins with DAVID database [30] and GO cluster enrichment analysis was carried using the top twenty significantly reduced or enriched GO terms with REVIGO web server [31].

2.12. Metabolomic and lipidomic analyses

The frozen tissues were ground on nitrogen and extracted as described [32]. The lipophilic extraction phase was used for LC-MS lipidomics analysis. The hydrophilic extraction phase was split to perform LC-MS and GC-MS metabolomic analysis. LC-MS measurements were performed using a Waters ACQUITY UPLC system (Milford, Massachusetts, USA) coupled to a Thermo Fisher QExactive mass spectrometer (Dreieich, Germany). Lipophilic compounds were separated using a C8 column and hydrophilic compounds using a C18 reverse phase column. The mobile phase composition and electrospray parameters were as described [32]. GC-MS measurements were performed as follows: An aliquot of the hydrophilic extraction phase was dried and the pellet was sequentially derivatized by methoxyamine/MSTFA and injected onto a DB35 GC column (Agilent Technologies GC, Waldbronn Germany) coupled to Leco Pegasus HT mass spectrometer with electron impact (EI) ionization source. Gas elution was performed for two minutes at 85 °C with a further temperature gradient of 15 °C per minute till a final temperature of 360 °C was reached. Peak-picking and background removal of the LC-MS data was accomplished with the Genedata REFINER MS® software (Basel, Switzerland). Chromatogram alignment and filtering were completed using in-house R-based software. Filtering included removal of isotopic peaks, in-source fragments, and additional lower intense adducts of the same analyte. The annotation of the content of the sample was accomplished by matching the extracted data from the chromatograms with our library of reference compounds in terms of accurate mass and retention time, and the most abundant adduct was used for relative quantification of a metabolite. GC-MS data were exported as NetCDF files from the Leco Pegasus software to "R". The package TargetSearch was used to transform retention time to retention index (RI), to align the chromatograms, extract the peaks, and annotate them by comparing the spectra and the RI to the reference database (Fiehn Lab Metabolomics, UC Davis, USA [33]). A unique mass was used to quantify relative concentrations of each identified metabolite. For those metabolites which were annotated in both GC-MS and LC-MS data, the value with smallest deviation was retained [32]. The VSCFA-TAG were identified in the MS2 frame of the mass spectrometer from the [M + NH₄]⁺ precursor in positive ionization mode. The fatty acids were identified on the basis of the AcylOOH + NH₃ neutral loss. The final composition was identified by comparison of the fatty acids present in the fragmentation frame to the theoretical composition of the precursor. [Supplementary Table 6](#) summarizes information on molecular masses of all VSCFA-TAG precursors, their theoretical composition and mass deviations from the theoretical mass. For every precursor, the fragments in the MS2 event of the data-dependent acquisition measurement (DDA) with corresponding relative abundance are presented. For every fragment a neutral loss corresponding to a fatty acid was calculated.

Unknown masses were re-annotated using Metlin database [34] and Lipidmaps structure database [35]. For identification of possible biomarkers, the slopes of age-dependent regressions were calculated and depicted as regression coefficient *r*. HeatMap was generated using ClustVis web tool [36].

2.13. Statistical analyses

Significance levels of differences between groups were evaluated using either an unpaired two-tailed Student's *t*-test, Mann-Whitney-U test or one-way analysis of variance (ANOVA) with Bonferroni *post-hoc* test.

3. RESULTS

3.1. BAT-aging is accompanied by impaired lipid metabolism

To establish the age-related defect of BAT-thermogenesis in our animal model, we analyzed *Ucp1* mRNA expression in BAT of young animals at 2.5 months of age compared to mice at 15 and 25 months of age. When housed at room temperature (RT, 22 °C), expression of *Ucp1* was decreased at 15 and 25 months of age (Figure 1A) and an increase of lipid droplet size in aged brown adipocytes was observed

(Fig. S1A). In inguinal WAT (iWAT) at room temperature, *Ucp1* levels were significantly reduced to 2.9% of young control levels only when comparing young mice to animals aged 25 months (Figure 1B). Since white fat expresses only low levels of *Ucp1* mRNA at room temperature, gene expression in iWAT was additionally tested after 7 days of incremental cold exposure. At 5 °C, the expression of *Ucp1* was strongly induced in all groups compared to room temperature, but a significant reduction of *Ucp1* mRNA was maintained in tissues from both groups of aged mice when compared to young controls

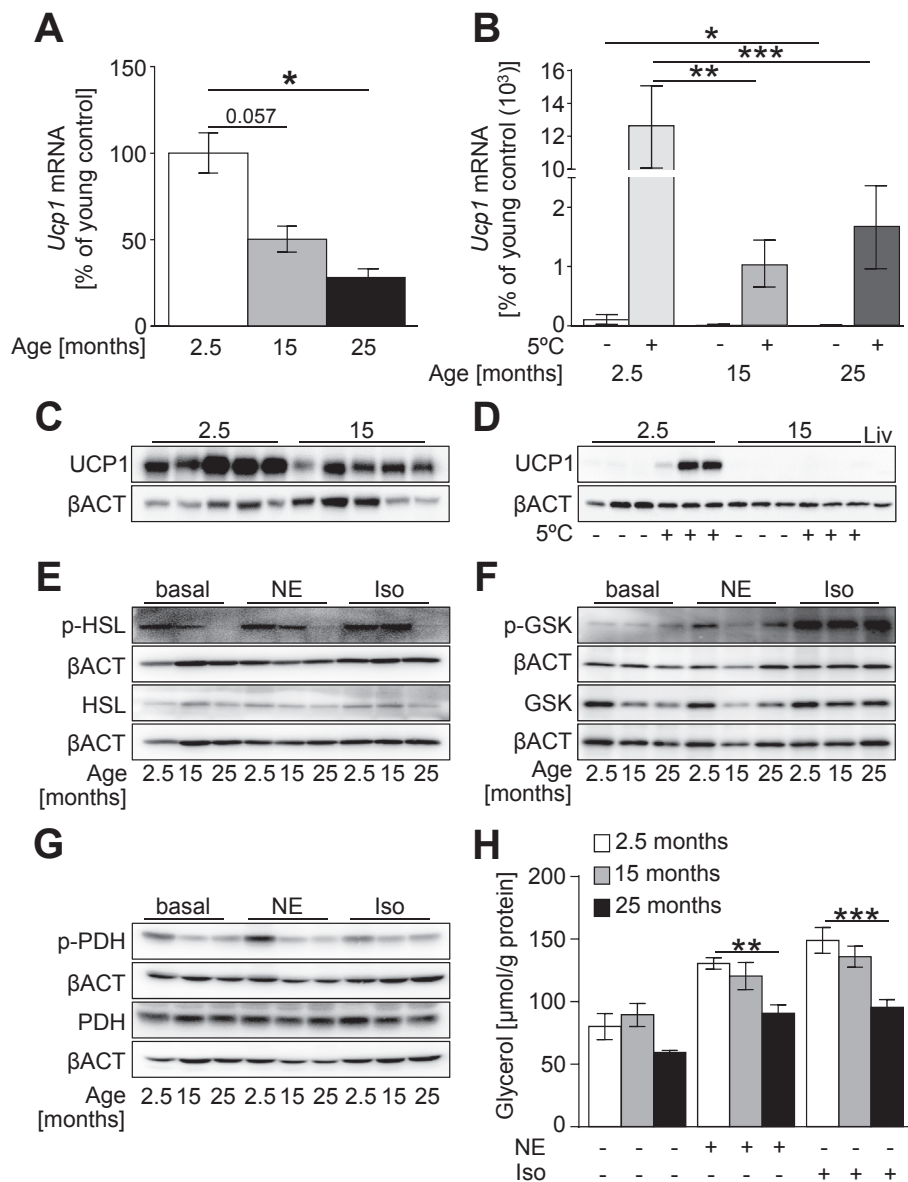


Figure 1: Age-related decline of lipid-related metabolism in BAT. (A) Analysis of *Ucp1* mRNA in interscapular BAT collected from mice of 2.5, 15, and 25 months of age. (B) Analysis of *Ucp1* mRNA in iWAT collected from mice of 2.5, 15, and 25 months of age with (+) and without (-) cold exposure. (C, D) UCP1 protein levels normalized to β-actin in BAT (C) and iWAT (D) collected from young (2.5 months) and old (15 months) mice (quantification: Figs. S1B and S1C). (E) Representative immunoblot image of phosphorylated HSL (p-HSL) and total HSL in BAT-explants isolated from young (2.5 months) and old (25 months) mice after normalization to β-actin (quantification: Fig. S1E). (F) Representative western blot image of phosphorylated GSK3β (p-GSK) and total GSK3β in BAT-explants isolated from young (2.5 months), middle aged (15 months), and old (25 months) mice after normalization to β-actin (quantification: Fig. S1F). (G) Representative immunoblot images of phosphorylated pyruvate dehydrogenase (p-PDH) and total PDH in BAT-explants isolated from young (2.5 months), middle aged (15 months) and old (25 months) mice after normalization to β-actin (quantification: Fig. S1G). (H) Glycerol [μmol/g protein] was measured in supernatant of adipose tissue explants using a photometric assay. Explants were treated for 2 h either with 10 μM norepinephrine (NE) or isoproterenol (Iso). The glycerol amount was normalized to explant protein content. Data are shown as mean ± SEM, n = 3–5; *p < 0.05; **p < 0.01; ***p < 0.001 using two tailed unpaired t-test or two way ANOVA.

(Figure 1B). Consistently, UCP1 protein was significantly reduced in BAT at 15 months of age and remained almost undetectable in aged iWAT after cold exposure, whereas UCP1 protein was readily induced in iWAT of young animals after cold (Figure 1C, D; Fig. S1B and S1C). To examine the effects of aging on adrenergic activation in BAT, we next analyzed expression of β 3-adrenergic receptor (*Adrb3*) mRNA, which was not changed significantly in BAT during aging (Fig. S1D). To determine whether aging impaired the signaling events controlling lipid mobilization in BAT, we next tested tissue-autonomous activation of lipolysis in BAT explants that were treated with norepinephrine (NE) or isoproterenol (Iso) to mimic local activation of β 3-adrenergic receptors. Under these conditions, we observed a significant reduction of hormone-sensitive lipase (HSL) phosphorylation in BAT of 15 and 25 months old mice (Figures 1E and S1E). Since lipolysis regulation is under control of protein kinase A (PKA) as the common downstream kinase of β 3-adrenergic signaling, we also determined phosphorylation of other PKA targets. Although the regulation was less pronounced compared to HSL, we also observed a trend of age-dependent reduction of inhibitory phosphorylation of glycogen synthase kinase 3 β (p-GSK3 β) following adrenergic stimulation (Figures 1F and S1F), as well as a significant reduction of inhibitory pyruvate dehydrogenase phosphorylation (p-PDH) in explants of 25 months old mice compared to 2.5 months old mice when stimulated with NE (Figures 1G and S1G). A potential explanation for the differences between phosphorylation of HSL and the other targets is that GSK3 β and PDH are also regulated by many other kinases that could affect their phosphorylation levels differentially. To more directly assess the effects of aging on lipid mobilization, we also examined lipolysis levels in the explants and observed a significant decrease of glycerol release from BAT explants of 25 months old mice after stimulation with norepinephrine or isoproterenol, which suggests reduced triglyceride hydrolysis during aging. These data support the conclusion of defective BAT thermogenesis during aging due to reduced beta adrenergic activity (Figure 1H).

To further investigate age-related defects in BAT, the proteomes of young and old BAT samples were compared by mass spectrometric analysis (Table S1). Pathway analyses using Kyoto Encyclopedia of Genes and Genomes (KEGG) annotation revealed, among others, a marked downregulation of pathways related to metabolic processes and pathways related to lipid homeostasis, as well as amino acid and carbohydrate metabolism to similar degrees (Figure 2A) in aging BAT while up-regulated pathways were less well defined and included ribosomal genes and, potentially, glucose metabolism processes (Figure 2B). To better define these pathways which are formed based on partially overlapping candidate genes, we used gene ontology (GO) term clustering which enriched several clusters after removal of redundant terms, including lipid homeostasis in the down-regulated pathway clusters (Figure 2C, Table S2) and processes related to immune and muscle function, among others, as up-regulated clusters in aging BAT (Figure 2D, Table S3). On the individual candidate protein level, proteins involved in lipid metabolism and mitochondrial function determined the clustering of down-regulated pathways (marked by blue arrows, Figure 2E, Table S4), while a group of myosin heavy chain family (MYH) proteins drove the up-regulated clusters (marked by red arrows, Figure 2F, Table S4).

3.2. Identification of potential lipid biomarkers of BAT aging

To examine age-related changes to lipid metabolism in brown adipose tissue, we analyzed age-dependent changes of metabolite levels in BAT. For metabolomic analysis, tissue samples were collected from BAT of mice at 2.5, 5, 10, 15, 21, and 25 months of age. The lipid

analysis resulted in the detection of a broad range of candidates, including many intermediate metabolites of biochemical processes but also a range of different lipids species (Table S5). When we selected candidates based on significant correlations with aging, 68 metabolites were identified, with 48 of them being different lipid species which could be roughly grouped into five distinct classes, including four carnitine-coupled fatty acids, 31 phospholipids, three sphingolipids, and ten triacylglycerols (Figure 3A, Table S5). Interestingly, among the triacylglycerols that showed a significant negative correlation to aging, four triacylglycerols containing very short chain fatty acids (VSCFA-TG) with two to five carbon atoms in their fatty acid moieties were detected. VSCFA-TAGs were identified in positive MS ionization mode from the $[M + NH_4]^+$ precursor with subsequent identification of fatty acid composition on the basis of AcylOOH + NH₃ neutral loss fragmentation (fragmentation patterns summarized in Table S6). This rare class of lipids, found to be much more abundant in BAT compared to iWAT, has not previously been described in BAT or WAT (Figure 3B, Table S7). Similarly, all four carnitines as well as the significantly changed triacylglycerols negatively correlated with aging (Figure 3C,D). Conversely, the majority of phospholipids, represented mainly by phosphatidylethanolamines (PE) and phosphatidylcholines (PC) as well as one sphingomyelin and two ceramide species, were positively associated with aging (Figure 3E,F). The increase of PEs and PCs was mainly driven by an increase in the amounts of unsaturated lipids, particularly in mice aged 21 and 25 months (Table S5). These changes in fatty acid compositions prompted us to more specifically investigate changes of fatty acid profiles in neutral lipid and phospholipid classes during aging which was conducted in samples of BAT and iWAT isolated from mice aged 2 and 12 months. Unexpectedly, the analysis of the fatty acid profiles in phospholipids as well as neutral lipids (including free fatty acids) by quantifying the amounts of saturated (SFA), monounsaturated (MUFA), polyunsaturated fatty acids (PUFA) showed only minor changes in BAT, whereas aging resulted in a shift towards desaturation of fatty acids in iWAT, which was detected with trends to reduction in SFA and significantly elevated levels of MUFA in iWAT (Fig. S2A–L, Table S8). To further evaluate the physiological relevance of changes to fatty acid composition, we also determined ratios of omega6 to omega3-fatty acids (ω 6/ ω 3) on both lipid classes. Here, aging resulted in significantly elevated ω 6/ ω 3 in iWAT-derived fatty acids from neutral as well as phospholipids, whereas the ω 6/ ω 3-ratio was only significantly induced by aging in neutral lipid-derived fatty acids in BAT (Fig. S2M–S2P).

Since several ceramides were elevated in aged AT, we next quantified ceramide subspecies using a targeted approach to measure individual ceramides with 16:0 to 24:0 fatty acid moieties. Consistent with our initial results from the non-targeted analysis, there was a significant accumulation of the ceramides C18:1, C20:0, C22:0 and C24:1 in aged BAT (Figure 4A) and of C18:1 and C20:0 in aged iWAT (Figure 4B), with the overall induction of ceramides being more pronounced in aged BAT.

A potential consequence of PE- and PC-upregulation in age-related dysfunction could be due to their effects on lipid biochemistry, for instance by increasing the catalytic activity of dolichol kinase [37]. This enzyme is highly expressed in BAT and phosphorylates dolichols, thereby bio-activating these lipid species for sugar-coupling as starting point of N-linked glycosylation. Dolichols have previously been described as biomarkers of aging in other tissues [38]. We therefore conducted a targeted measurement of different dolichols in BAT and iWAT of young and aged mice by HPLC. Similar to what was previously described in other tissues, a significant increase was observed for all identified dolichol species ranging from 16 to 20 isoprene backbone

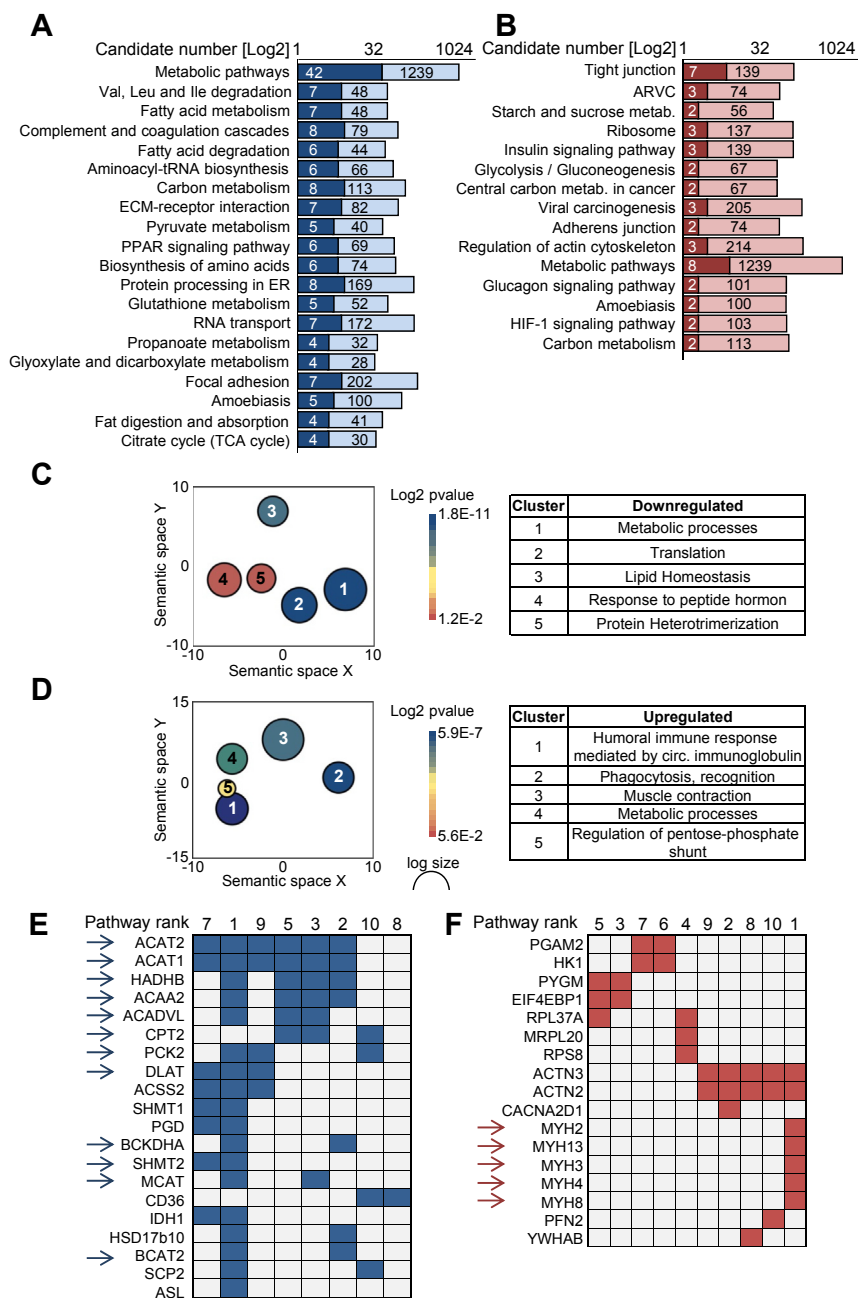


Figure 2: Aging results in defective adipose tissue lipid metabolism. (A) Pathway clustering for 180-proteomic analysis of aged BAT. Detected proteins that were reduced in aged mice were identified based on heavy/light ratios (H/L ratio) < 1 to identify panels of potentially age-sensitive protein clusters that were annotated to appropriate pathways based on KEGG classification. Candidates were chosen from two independent experiments executed as forward and reverse experiments, either labeling proteins from young or aged BAT with 18O. Each sample was generated by pooling protein extracts from five animals per age-group (Table S1). Significantly enriched pathway clusters were identified based on p-values < 0.05 and first twenty pathways are depicted in logarithmic scale (candidate protein number in pathway expressed in binary logarithmic scale [log2]) in which light blue indicates total number of genes in pathway and dark blue indicates number of identified proteins in pathway. (B) Pathway clustering for proteins enriched in aged BAT samples by 18O-labeled proteomic analysis. Proteins were identified based on heavy/light ratios (H/L ratio) > 2.5 and were annotated to appropriate pathways based on KEGG classification. Candidates were chosen from two independent experiments executed as forward and reverse experiment, either labeling proteins from young or aged BAT with 18O. Each sample was generated by pooling protein extracts from five animals per age-group (Table S1). Significantly enriched pathways were identified based on p-values < 0.05 and depicted in logarithmic scale (candidate protein number in pathway expressed in binary logarithmic scale [log2]) in which light red indicates total number of genes in pathway and dark red indicates number of identified proteins in pathway. (C, D) Gene ontology (GO) cluster enrichment analysis was carried out to group redundant GO terms using the top twenty significantly reduced (C) or enriched (D) GO terms using the REVIGO web server. Bubble size and color define frequency (log value) of the GO term and significance levels, respectively (for GO Term list see Tables S2 and S3). Semantic space describes the relatedness degree between two annotation entities. Annotated clusters based on GO term grouping are listed in tables on right. (E) Clusterogram of downregulated individual and overlapping proteins of the different GO pathways listed in panel A (for explanation of gene name abbreviations see Table S4A). Blue arrows indicate candidates belonging to the lipid homeostasis cluster (pathways of fatty acid metabolism and degradation) as well as mitochondrial genes. (F) Clusterogram of upregulated individual and overlapping proteins of the different GO pathways listed in panel B (for explanation of gene name abbreviations see Table S4B). Red arrows indicate candidates belonging to the myogenic gene cluster.

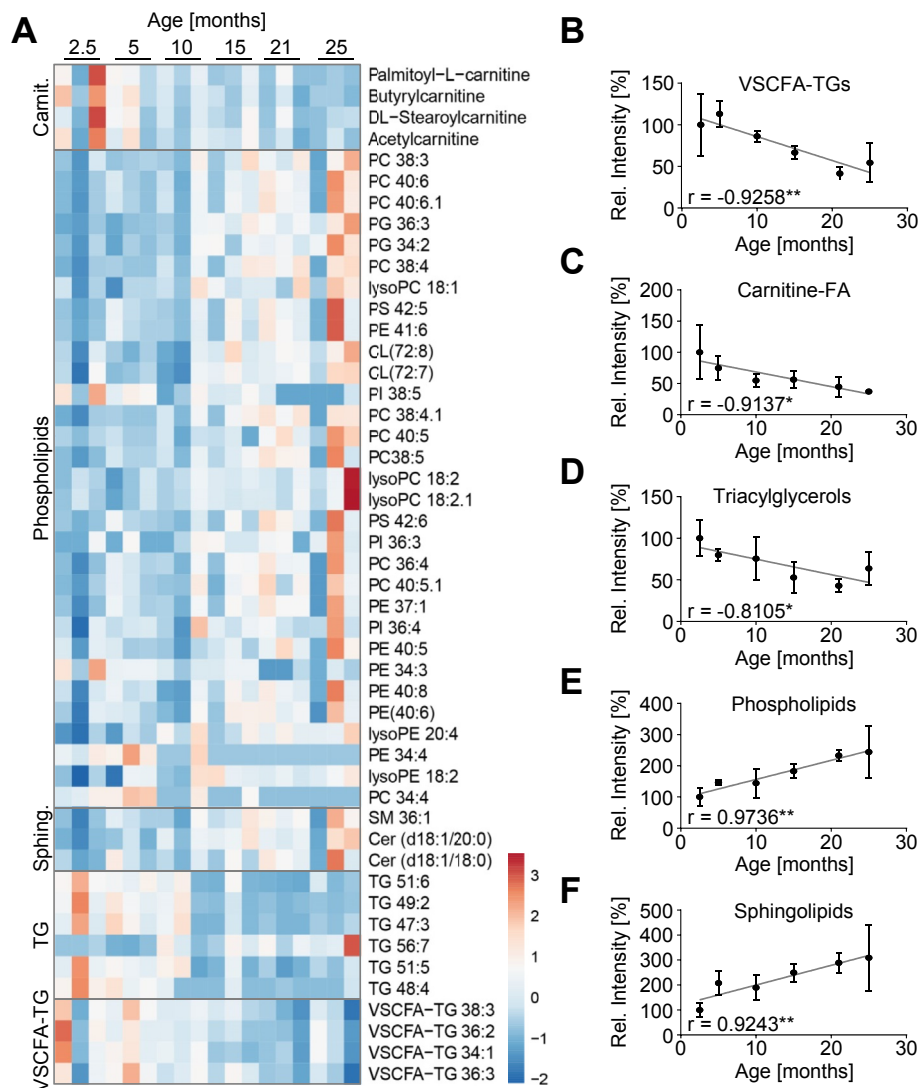


Figure 3: Metabolomic analysis of BAT reveals age-related changes of several lipid classes. (A) HeatMap of lipids metabolites with relative intensities determined by LC-MS showing significant correlations in BAT as a function of aging in animals aged 2.5, 5, 10, 15, 21, and 25 months. Correlation coefficients (r) for individual lipids were calculated and lipids showing significant ($p < 0.05$) correlations to age were grouped into lipid classes, i.e. carnitine-bound fatty acids (Carnit.), phospholipids, sphingolipids including ceramides (Sphing.), triacylglycerols (TG), and triacylglycerols containing very short chain fatty acids (VSCFA-TG). Heatmap was generated using ClustVis, elevated relative values are depicted in red, low relative values are depicted in blue (Candidate list and data used for heat map generation are summarized in suppl. Table S5). (B–F) Lipids shown in the heatmap (panel A) were clustered into lipid classes to visualize age-dependent correlations of lipid classes: Very short chain fatty acids containing-TGs (B, Tables S6 and S7, VSCFA-TG; $p = 0.0081$), carnitine-bound fatty acids (C, Carnitine-FA; $p = 0.0109$), triacylglycerols (D; $p = 0.0505$), phospholipids (E; $p = 0.0010$) and sphingolipids (F; $p = 0.0084$). For panels B–F, the average correlation values of all individual candidates' correlations with age were calculated. To this end, individual peak intensities of all age groups were normalized to intensities measured in young control group (age: 2.5 months). Data are depicted as mean \pm SEM ($n = 3$ group); * $p < 0.05$; ** $p < 0.01$ using two tailed unpaired t-test.

units in BAT of aged animals (Figure 4C). In line with this result, we also detected an accumulation of dolichols in iWAT, although the overall amount of dolichols, when normalized to total protein, was lower in iWAT compared to BAT (Figure 4D).

3.3. Ceramides attenuate differentiation of brown pre-adipocytes

To assess the biological effects of ceramides on brown adipocyte metabolism, we treated an immortalized brown pre-adipocyte cell line with ceramide C16 during adipogenic differentiation. Under these conditions, expression of brown adipocyte marker genes, *Ucp1* and peroxisome proliferator-activated receptor gamma coactivator 1-alpha (*Ppargc1 α*), and the adipokine Leptin (*Leptin*) were reduced in cells exposed to ceramide, while expression of a general adipogenic

marker, peroxisome proliferator-activated receptor gamma (*Pparg*), was not changed (Figure 5A). Conversely, exposure of differentiating brown pre-adipocytes to fumonisins B1 (FB1), an inhibitor of ceramide synthesis, induced expression of adipogenic genes, including cell death activator CIDE-A (*Cidea*), *Pparg* and Perilipin-1 (*Plin1*), while *Ucp1*, *Ppargc1 α* and *Leptin* mRNAs were not affected (Figure 5B). To reproduce these observations in a different cell model, we repeated similar experiments with primary adipogenic progenitor cells (APCs) freshly isolated from brown adipose tissue by flow cytometry. Gene expression analysis of primary APCs treated with ceramide C16 during differentiation confirmed the negative effects of this ceramide on (brown) adipogenic differentiation by showing a significant down-regulation of several brown adipocyte-specific marker genes

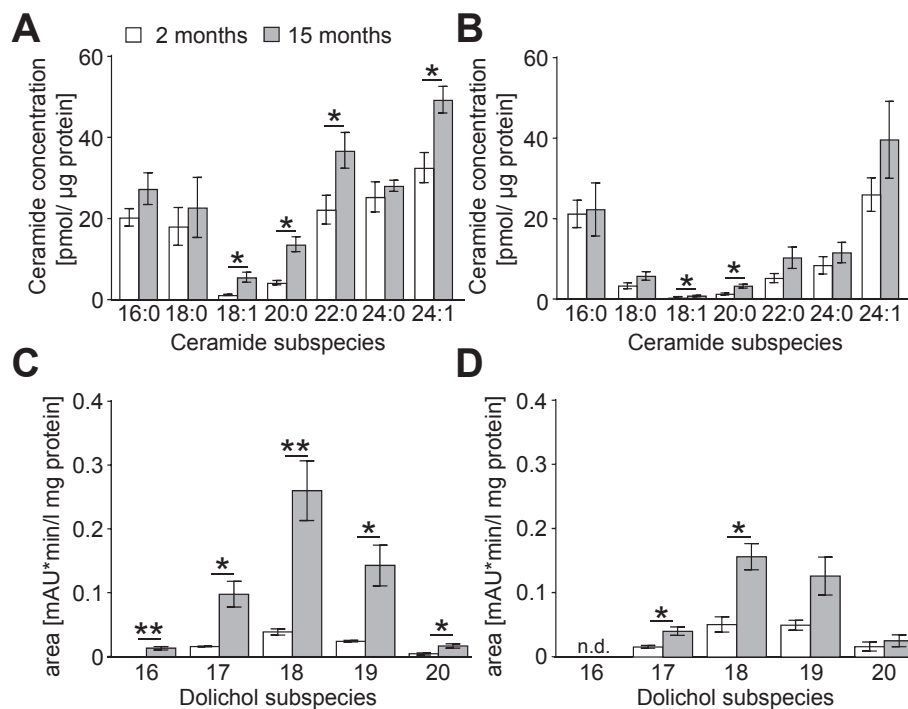


Figure 4: Targeted lipidomic analysis of ceramides and dolichols as potential biomarkers of BAT-age. (A, B) Targeted mass spectrometric analysis of tissue ceramides using QTOF MS in young (2 months; white bars) and aged (15 months; gray bars) BAT (A, n = 10) or iWAT (B, n = 5). Ceramides were identified by their accurate mass-to-charge ratios (m/z) and characteristic MS/MS fragmentations and quantified based on peak area quantification and normalized to samples' protein content. (C, D) HPLC-based analysis of dolichol subspecies with increasing length of isoprenoid side chains from 16 to 20 subunits in young (2 months; white bars) and aged (15 months; grey bars) BAT (C, n = 5) or iWAT (D, n = 5). Individual dolichols were identified after comparison to standards and quantified based on peak area quantification and normalized to samples' protein content. Data are shown as mean \pm SEM; * p < 0.05; ** p < 0.01 using two-tailed unpaired t-test.

(Figure 5C), general adipogenic genes (Figure 5D), and markers of mitochondrial biogenesis (Figure 5E). In accordance with the altered gene expression patterns, mitochondrial respiration was reduced in the brown pre-adipocyte cell line upon exposure to ceramides throughout differentiation (Figure 5F,G). Comparable to the expression profile in immortalized brown pre-adipocytes treated with FB1 (Figure 5B), exposure of primary APCs to FB1 resulted in an induction of brown adipogenic marker genes, while conversely gene expression of the adipogenic marker *Leptin* was significantly decreased and no changes of *Pparg* and *Plin1* expression were measured (Figure 5H,I). The beneficial effect of ceramide synthase inhibition by FB1 was further confirmed by elevated expression of mitochondrial genes (Figure 5J). Lastly, to test whether ceramides were also able to acutely affect more mature brown adipocyte stages, we exposed immortalized pre-adipocytes to ceramide C16 for the final 48 h of the differentiation time course. Similar to the full-time treatment, *Ucp1* mRNA was reduced under basal conditions and 48 h ceramide administration attenuated the isoproterenol-induced expression of *Ucp1*, whereas expression of *Pparg* as a general differentiation marker was not affected (Fig. S3A, B). In line with this observation, mitochondrial respiration and uncoupling of brown adipocytes was also significantly reduced by short-term ceramide exposure (Fig. S3C, D).

3.4. Sphingosine 1-phosphate signaling inhibits brown adipocyte function

Ceramides can be converted into sphingosine 1-phosphate (S1P) by ceramidases and subsequent phosphorylation by sphingosine kinase [39], and an age-related increase in ceramides could thereby also affect this lipid-based signaling molecule. Binding of S1P to its G-

protein coupled receptors mediates pleiotropic effects in different cell types and very little is known about their role in regulating brown adipocyte formation and function. We therefore treated primary brown APCs with increasing concentrations of S1P during differentiation, which was combined with or without short-term adrenergic stimulation by NE. While the treatment with S1P had no effect on the expression of *Ucp1* (Figure 6A) or *Pparg1a* (Figure 6B) under basal conditions, a dose-dependent attenuation of NE-stimulated gene expression was detected during co-exposure to S1P, altogether suggesting a negative effect of S1P on brown adipogenesis. To determine the relative contribution of the different receptors on S1P-signaling in adipogenic cells, we next compared expression of all five receptor types in adipose tissue and purified APCs of BAT and iWAT. Sphingosine 1-phosphate receptor type 1 (*S1pr1*), *S1pr4*, and *S1pr5* were expressed in both types of adipose tissue at higher levels compared to the respective APC-isolates. Conversely, *S1pr2* and *S1pr3* were equally expressed in APCs and whole tissue (Figures 6C, S4A–C). We next used specific antagonists to specifically inhibit receptors during adipogenic differentiation, using either VPC23019 (VPC) to target S1P receptor types 1 and 3 (S1PR1, 3) simultaneously, S1PR2 by using JTE013 (JTE), or S1PR4 by using CYM50358 (CYM). Under these conditions of reduced S1P-signaling, *Ucp1* expression was significantly induced in cells treated with antagonists of S1PR2 (JTE) and S1PR4 (CYM), whereas no effects on expression of adipogenic differentiation marker *Pparg* were detected by any of the inhibitors (Figure 6D). Although *S1pr3* expression was expressed in APCs to the same extent as in whole tissue (Fig. S4B), no effect of the antagonist on brown adipogenesis was detected (Figure 6D). *S1pr2* was found to be highly expressed in adipose tissue and APCs whereas *S1pr4* was highly expressed in

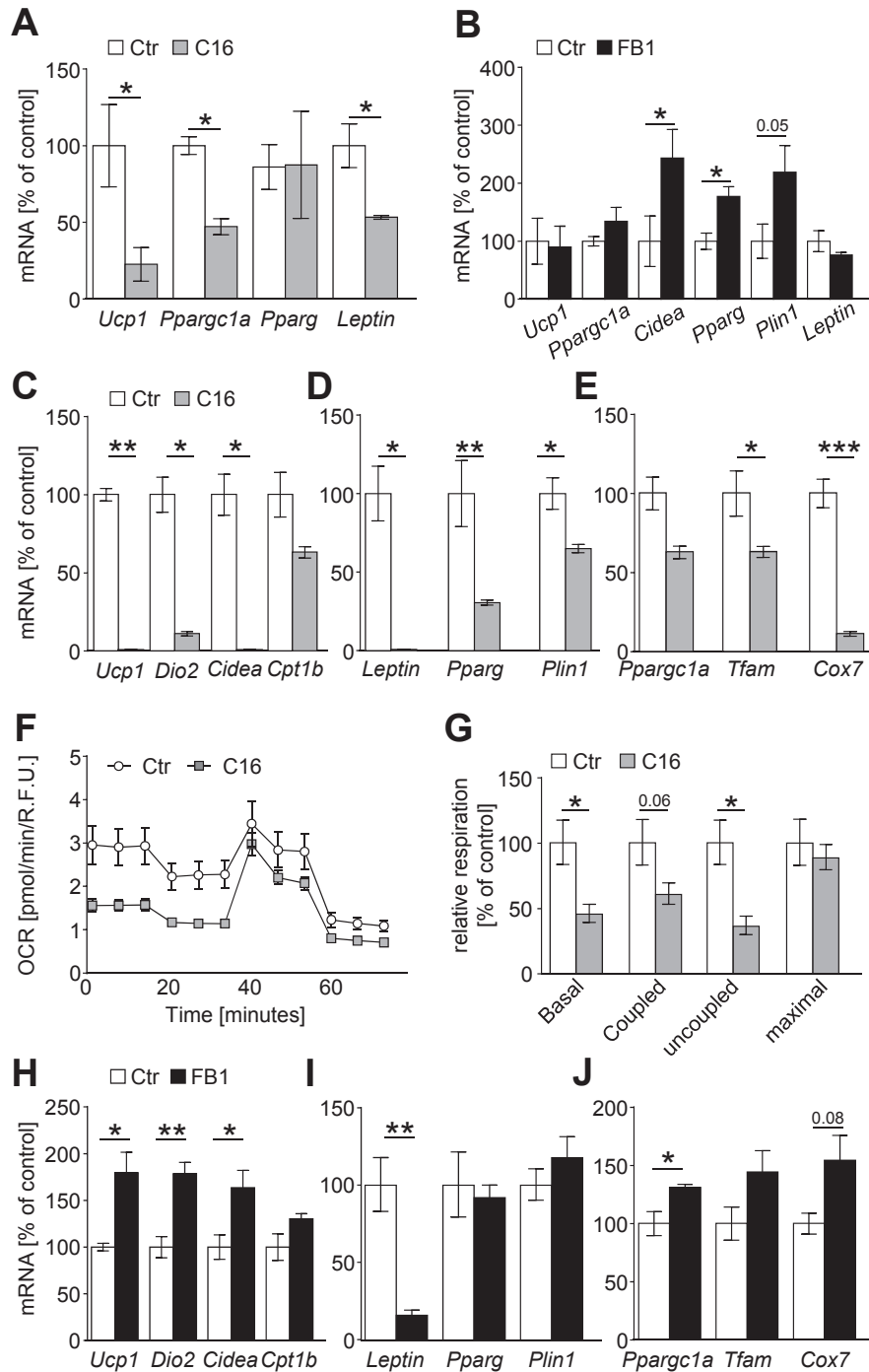


Figure 5: Ceramides impair adipogenic differentiation of brown pre-adipocytes. (A) mRNA levels of adipocyte specific genes in immortalized brown pre-adipocyte cell line WT1 treated with 10 μ M of C16 ceramide (gray bars) or solvent control (white bars) during differentiation. (B) mRNA levels of brown adipogenic genes in immortalized brown pre-adipocyte cell line WT1 treated with solvent control (white bars) or 5 μ M of ceramide synthase inhibitor fumonisins B1 (black bars) during adipogenic differentiation. (C, D, E) Primary adipogenic progenitor cells (APCs) were isolated from BAT by flow cytometry. mRNA levels of brown adipocyte marker genes (C), general adipocyte-specific genes (D), and genes of mitochondrial biogenesis (E) in primary APCs treated with control (white bars) or C16 ceramide (10 μ M; gray bars) during differentiation. (F, G) Analysis of mitochondrial respiration in immortalized brown WT1 pre-adipocytes differentiated under adipogenic conditions for 10 days comparing control (Ctr; white circles, white bars) to cells treated with C16 ceramide throughout differentiation (C16; gray squares, gray bars). Oxygen consumption rates were recorded (F) and normalized to DAPI staining (relative fluorescence units, R.F.U.) for quantification (G; n = 6). Basal respiration rate measurements were followed by administration of oligomycin (after third time point) to determine ATP-linked (coupled) respiration. Maximal respiration capacities were measured after FCCP-administration (after sixth time point) and non-mitochondrial respiration was measured by adding rotenone and antimycin A (after ninth time point). Uncoupled, e.g. potentially UCP1-dependent proton leak, was calculated from the relative differences of respiration rates after oligomycin and rotenone/antimycin A. (H, I, J) Primary adipogenic progenitor cells (APCs) were isolated from BAT exposed to control conditions (white bars) or ceramide synthase inhibitor fumonisins B1 (5 μ M; black bars) during differentiation. Data are shown as mean \pm SEM (n = 3–6); *p < 0.05; **p < 0.01; ***p < 0.001 using two tailed unpaired t-test or one-way ANOVA.

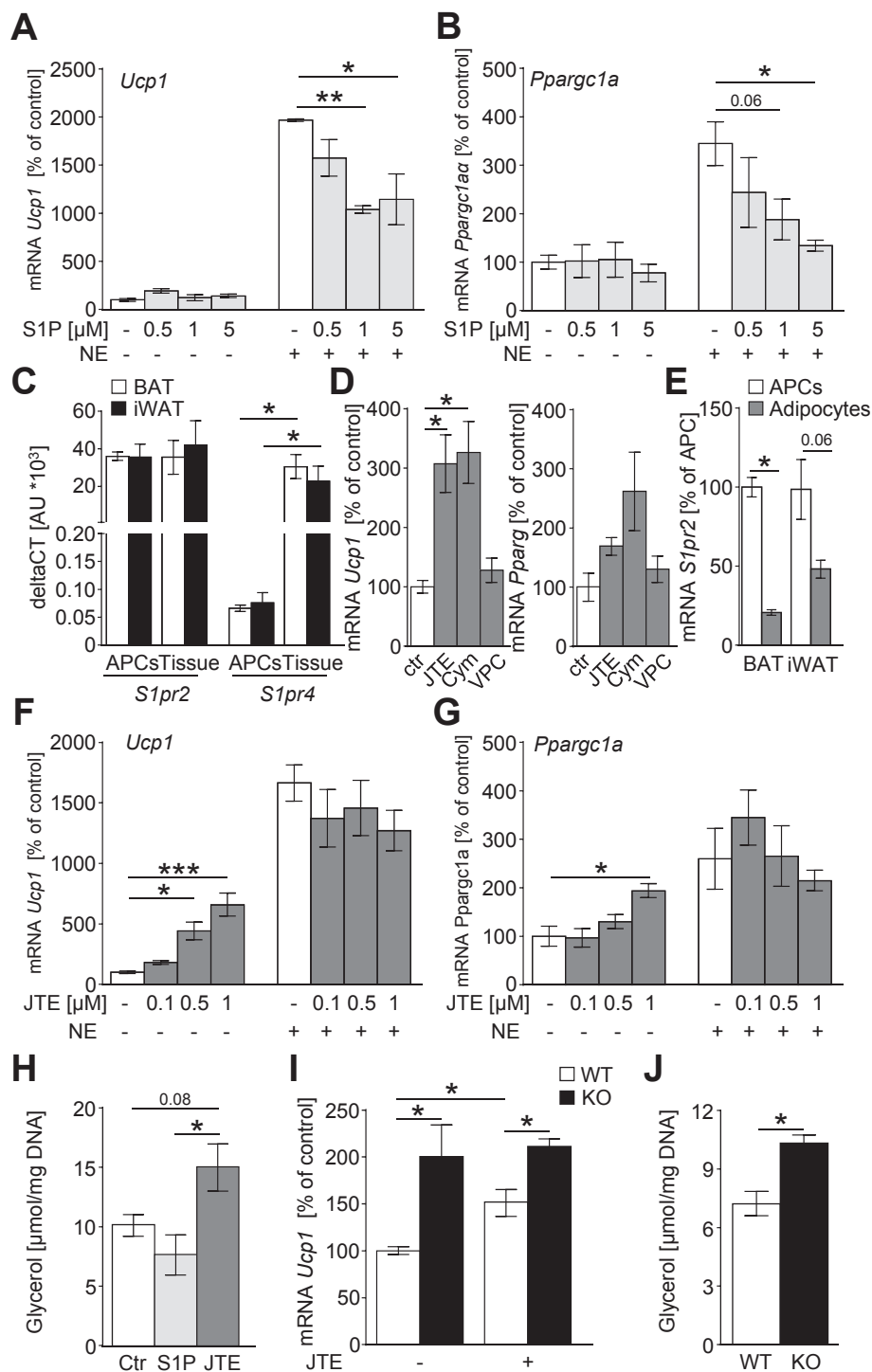


Figure 6: The sphingolipid S1P inhibits brown adipocyte formation and function. (A, B) mRNA levels of *Ucp1* (A) and *Ppargc1a* (B) in primary brown APCs treated with increasing concentrations of S1P during differentiation without (white bars) or after a 4 h treatment with NE (lights gray bars) prior to cell harvest. (C) Comparison of *S1pr2* and *S1pr4* mRNA expression in APCs isolated from BAT (white bars) and iWAT (black bars) or whole brown and subcutaneous white adipose tissue (Analysis of *S1pr1*, *S1pr3*, and *S1pr5*: Fig. S4). (D) Gene expression analysis in APCs treated with solvent control (white bars) or inhibitors (dark gray bars) targeting S1PR2 (JTE), S1PR4 (Cym), and a combined inhibitor targeting S1PR1 and S1PR3 (VPC) throughout differentiation (all at 1 μM). (E) *S1pr2* mRNA expression in undifferentiated APCs (white bars) compared to mature adipocytes (black bars) after 12 days of *in vitro* differentiation. (F, G) mRNA levels of *Ucp1* (F) and *Ppargc1a* (G) in APCs treated with solvent control (white bars) or increasing concentrations of S1PR2-inhibitor (JTE; gray bars) during differentiation without or with 4 h treatment with NE before harvest. (H) Lipolysis rates as measured by glycerol release from *in vitro* differentiated primary brown adipocytes treated either with solvent control (white bar), 1.0 μM S1P (light gray bar), or 1.0 μM JTE (dark gray bar). (I) *Ucp1* mRNA expression in *in vitro* differentiated APCs isolated from wildtype (WT, white bars) or *S1pr2*-knockout mice (KO, black bars) without treatment (-) or exposed to 1 μM JTE (+) during differentiation. (J) Norepinephrine-stimulated glycerol release from primary adipocytes differentiated after isolation from wildtype mice (WT, white bars) or *S1pr2*-deficient mice (KO, black bars). Data are shown as mean ± SEM, n = 3; *p < 0.05; **p < 0.01; ***p < 0.001 using two tailed unpaired t-test.

whole adipose tissue but not in APCs (Figure 6C). Due to its particularly high expression in APCs and the induction of *Ucp1* following S1PR2-inhibition, we concluded that *S1pr2* may be the most relevant subtype to control brown adipocyte progenitor cells. Consistent with this hypothesis, *S1pr2*-mRNA was expressed at lower levels in mature adipocytes compared to APCs from BAT as well as iWAT (Figure 6E). To further test the role of this receptor in brown adipocyte formation, APCs were incubated with increasing concentrations of JTE during differentiation, which led to a dose dependent increase of BAT marker genes *Ucp1* and *Ppargc1a* in these cells without adrenergic stimulation. Of note, the effects of S1PR2 inhibition were more potent when cells were exposed at later time windows during the differentiation time course, while no or very little effect was observed when cells were only treated before or in the early phases of adipogenesis, which may indicate that altered S1P-signaling is required throughout differentiation to impact brown adipogenesis (Fig. S4D, E). JTE treatment also yielded no additional benefit in cells stimulated with NE for 4 h before harvest, suggesting that both compounds may act on the same pathway, i.e. the signaling cascade downstream of adrenergic receptors (Figure 6F,G). Consistent with this assumption, an increase of glycerol release as a measure of lipolytic activity was observed in cells exposed to JTE, but not S1P (Figure 6H).

To recapitulate the beneficial effects of loss of S1PR2 signaling on brown adipogenesis, we analyzed *Ucp1* expression in primary APCs isolated by flow cytometry from BAT of *S1pr2* knock-out mice which were differentiated under normal adipogenic conditions or in combination with JTE-exposure. Genetic ablation of *S1pr2* yielded the expected increase in *Ucp1* mRNA in knockout-cells when compared to cells isolated from wildtype littermates, which was also observed in wildtype cells exposed to JTE (Figure 6I). No additional induction was found for the combination of gene deletion and JTE-exposure, suggesting that JTE specifically acts on S1PR2 (Figure 6I). Similarly, glycerol release was elevated in cultured adipocytes from *S1pr2*-knockout mice compared to wildtype adipocytes (Figure 6J). Taken together, these data show that S1P-signaling influences brown adipogenesis, potentially by manipulating G-protein coupled signaling cascades.

3.5. Functional implications of dolichols as biomarkers for brown adipose tissue aging

Using a targeted quantification approach, we confirmed the previously detected age-dependent accumulation of dolichols in BAT. Dolichols are synthesized by the mevalonate pathway where the initial step is catalyzed by the enzyme HMG-CoA reductase (*Hmgcr*). The resulting products are precursors of cholesterol as well as dolichol synthesis [40]. In support of elevated dolichol levels, expression of several enzymes of the mevalonate pathway was upregulated in aged BAT (Figure 7A) whereas only dehydrololichyl diphosphate synthase (*Dhdds*) was upregulated in aged iWAT (Figure 7B). The final step of the synthesis of biologically active dolichols is the phosphorylation by dolichol kinase (*Dolk*), an enzyme that is highly expressed in BAT compared to other tissues [41]. To determine the function of dolichol kinase in brown adipocyte formation and metabolism, we generated progenitor cell lines stably overexpressing *Dolk* (Figure 7C,D). Confirming the potential negative effect of *Dolk* on brown adipogenesis, its over-expression was accompanied by reduced triglyceride accumulation (Figs. 7E and S5A). In accordance with these observations, lower expression of *Ucp1* mRNA was detected in *Dolk*-expressing adipocytes before and after stimulation with NE (Figure 7F). Subsequent functional analyses showed that excess *Dolk* expression attenuated glycerol release, indicating less efficient lipolysis in *Dolk* overexpressing cells

(Figure 7G), and reduced coupled and uncoupled mitochondrial respiration, although maximal respiration capacity was unchanged compared to control cells (Figure 7H,I). To further investigate the effects of dolichol kinase, we examined adipogenic progenitor cells isolated from a mouse model with heterozygous inactivation of the *Dolk* gene (HET), since homozygous gene deletion resulted in embryonic lethality. *In vitro* differentiated primary adipocytes FACS-isolated from HET mice displayed reduced DOLK protein levels (Figures 7J and S5B). Moreover, expression of *Ucp1* mRNA was increased in adipocytes differentiated from BAT- and iWAT-derived primary APCs following NE stimulation (Figure 7K, L), which was confirmed on the UCP1 protein level for BAT-derived primary ACPs after differentiation (Figures 7M and S5C).

4. DISCUSSION

Metabolic processes in brown and white adipose tissue play key roles in energy homeostasis. Here we show that aging results in defective lipid metabolism in BAT and WAT on the functional and the proteome level by targeting the ability of brown adipocytes to mobilize lipids after adrenergic stimulation. Exploring this observation, we identify several potential lipid species that may be used as biomarkers of the functional decline of brown adipocytes during aging, including very short chain fatty acid-containing triglycerides, sphingolipids, and dolichols. As a functional consequence of age-related alterations of these biomarkers, ceramides and their metabolic product, S1P, attenuate differentiation of brown pre-adipocytes and attenuate their metabolic function, in part due to S1P receptor activation. Similarly, elevated dolichol metabolism and increased expression of dolichol kinase may exacerbate metabolic defects by inhibiting brown adipocyte formation and function. Reduced BAT mass, lower thermogenic capacity, and the inability of WAT to undergo cold-induced browning have all been described in rodent and human aging [5,10,42]. On the molecular level, this may be due to reduced expression of the unique brown adipocyte marker *Ucp1*, reduced pre-adipocyte activation and differentiation or an attenuated adrenergic response to cold [8,9]. The age-dependent decrease of adipose tissue hormone-sensitivity [43] could be related to molecular changes within the adipocytes themselves, rather than the reduced adrenergic stimulus since circulating norepinephrine is elevated, rather than decreased, in cold-exposed aged rats compared to young controls [9]. However, the sympathetic stimulus at the tissue level may be unrelated to circulating norepinephrine and could be related to a changed quality of neuronal input to BAT during aging. Related to this, we observed increased expression of myogenic markers in aged BAT in our study. This effect is potentially comparable to a recent study where activation of AgRP-neuron activity changed the transcriptional profile of brown fat towards elevated expression of a wide array of myogenic genes and was linked to impaired BAT function [44]. Whether the age-dependent increase of myogenic marker expression is to some extent related to changes of AgRP-neuron activity remains to be elucidated. In summary, it is clear that multiple mechanisms may contribute to aged BAT dysfunction. The composition of the local microenvironment as well as endocrine and neuronal signals acting on brown adipogenic stem cells or mature brown adipocytes may provide key elements of this negative regulation. Secondly, since brown adipocytes do not normally occur as a pure population, especially in humans, biomarkers representing the number of brown adipocytes and their ability to conduct thermogenesis are of particular interest to test clinical applications. We here show that several lipid species may fulfill these prerequisites while also exerting regulatory impulses on brown adipocytes. Of particular interest is a

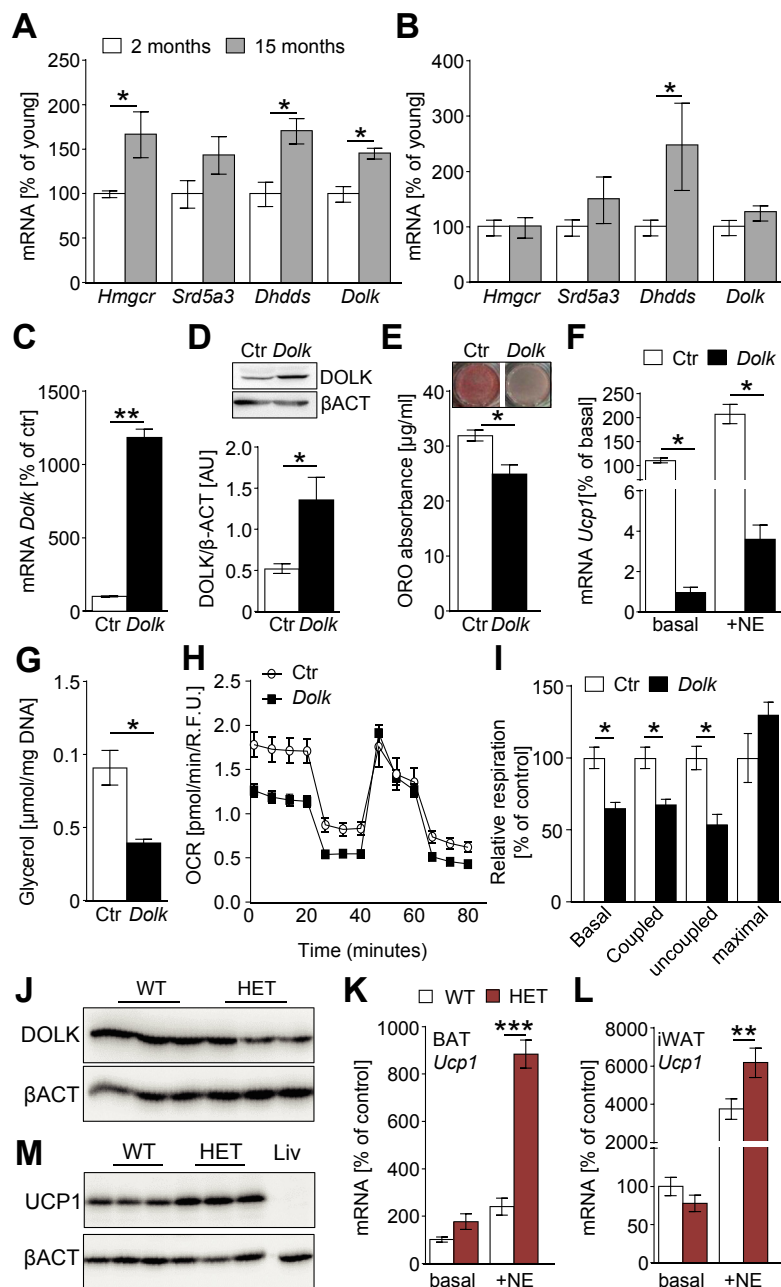


Figure 7: Dolichol metabolism regulates brown adipocyte function. (A, B) Gene expression analysis of enzymes catalyzing dolichol synthesis: HMG-CoA-reductase (*Hmgcr*), steroid 5 alpha reductase (*Srd5a3*), dehydrololichyl diphosphate (*Dhdds*) and dolichol kinase (*Dolk*) in BAT (A) and iWAT (B) isolated from young (2.5 months, white bars) and old (15 months, gray bars) mice. (C) *Dolk* mRNA expression in *Dolk*-overexpressing immortalized WT1 pre-adipocytes (black bars) differentiated for ten days compared to control cells (Ctr, white bars). (D) DOLK protein detection in undifferentiated cells stably overexpressing *Dolk* or control cells (Ctr) (upper panel). Quantification of signal intensity of three independent blots with normalization to β-actin (lower panel) of control cells (white bar) compared to *Dolk*-overexpression (black bars). (E) Oil Red O staining (upper panel, magnifications in Fig. S5A) and quantification after staining of mature control adipocytes (left; white bar) or cells with *Dolk*-overexpression (right; black bar) differentiated for 10 days. (F) *Ucp1* mRNA in *Dolk*-overexpressing pre-adipocytes (black bars) differentiated 10 days compared to control (white bars) without (basal) or with a 4 h norepinephrine (+NE) stimulation. (G) Norepinephrine-stimulated glycerol release from *Dolk* overexpressing immortalized pre-adipocyte cell line differentiated for 10 days (*Dolk*, black bars) compared to control cells (Ctr, white bars) normalized to total DNA content. (H, I) Analysis of mitochondrial respiration in immortalized control (Ctr) or *Dolk*-overexpressing (*Dolk*) brown WT1 pre-adipocytes differentiated under adipogenic conditions for 10 days. Oxygen consumption rates were recorded (H) and normalized to DAPI staining (relative fluorescence units, R.F.U.) for quantification (n = 12) (I). Basal respiration rate measurements were followed by administration of oligomycin (after third time point) to determine ATP-linked (coupled) respiration. Maximal respiration capacities were measured after FCCP-administration (after sixth time point) and non-mitochondrial respiration was measured by adding rotenone and antimycin A (after ninth time point). Uncoupled, e.g. potentially UCP1-dependent proton leak, was calculated from the relative differences of respiration rates after oligomycin and rotenone/antimycin A. (J) DOLK protein in differentiated APCs isolated from BAT of wild type (WT) or heterozygous *Dolk* knockout (HET) mice after 4 h NE stimulation after normalization to β-actin (Quantification: suppl. Fig. S5B). (K, L) mRNA expression levels of *Ucp1* in differentiated APCs isolated from BAT (K) or iWAT (L) tissue of wild type (WT; white bars) or heterozygous *Dolk* knockout mice (HET; red bars) after 12 days of differentiation without (basal) or after 4 h NE stimulation (+NE). (M) UCP1 protein levels in brown adipocytes of wild type (WT) and heterozygous knockout (HET) mice after normalization to β-actin (Quantification: suppl. Fig. S5C). Data are shown as mean ± SEM, n = 3–12; *p < 0.05; **p < 0.01; ***p < 0.001 using two tailed unpaired t-test or Mann-Whitney-U test.

relatively unusual group of triglycerides incorporating very short chain fatty acids (VSCFA), such as acetate (C2) and butyrate (C4). To our knowledge, the comparably high abundance of these triglyceride species in BAT compared to WAT, and their inverse correlation to age, have not previously been reported. This subgroup of fatty acids is produced mostly in the gastrointestinal tract by bacterial fermentation. After absorption, VSCFA are taken up by peripheral tissues and could directly impinge on energy metabolism by activation of the short chain fatty acid-activated G-protein coupled receptors GPR41 and GPR43 [45]. Notably, sodium acetate has also been shown to decrease phosphorylation of hormone sensitive lipase in 3T3L1 (white) adipocytes [46] and the inhibition of lipolysis by short chain fatty acids has been confirmed in humans as well as other experimental systems [47]. Loss of GPR43 also benefits metabolic health by increasing energy expenditure, improving glucose control and instating resistance to diet-induced obesity [48]. It is currently unknown whether short chain fatty acids are incorporated into triglycerides through the same mechanism as longer-chain fatty acids. In this study, we identified 20 such lipid species, of which several were significantly down-regulated by aging, containing either acetate or butyrate with high abundance in BAT in comparison to iWAT, thereby making VSCFA-TGs possible biomarkers of BAT aging. It remains to be determined whether VSCFA-TGs are solely biomarkers or may influence brown adipocyte thermogenesis by activating distinct signaling pathways due to controlled release of short chain fatty acids.

In our analysis, different types of phospholipids are, in general, positively correlated with aging. Phospholipids, and particularly phosphatidylethanolamines and phosphatidylcholines, are the main components of biological membranes and regulate membrane fluidity of eukaryotic cells [49]. While it is difficult to link such associations directly to changes in membrane function or other cellular processes involving phospholipids, some studies at least suggest that age-related changes to distinct phospholipids species also occur in other contexts. Increased levels of ether-phospholipids, but not total phospholipids, and elevated desaturation in PL-bound fatty acids have previously been described for visceral white adipose tissue [50], which is consistent with the hypothesis of altered membrane fluidity, thickness and mechanical resistance [51] and may also be related to increased adipocyte size in aged tissue samples. While the changes to fatty acid profiles are generally consistent with our own data from iWAT, the changes in BAT seem generally milder, which could be due to the age at which fatty acids profiles were assessed. Interestingly, the role of acyl-carnitine metabolism could also be related to these observations. Among the classes of lipids down-regulated by aging, we observed several fatty acid-carnitine conjugates, which are involved in fatty acid transfer into mitochondria through the carnitine acyltransferase system. Of note, phospholipids are also downregulated in aging heart mitochondria and treatment of such mitochondria with acetyl-carnitine reverted this negative effect of aging, suggesting a potential mechanistic link between alterations in phospholipids and acyl-carnitine metabolites [52]. In line with these observations, the ratios of ω 6/ ω 3 fatty acids in phospholipids became more unfavorable in aged BAT and iWAT, a development that has also been linked to metabolic disorders [53].

A metabolic connection between phospholipids, specifically phosphatidylcholines, and sphingolipids is well established. Our findings show that enrichment of ceramides in aged BAT and iWAT impairs brown adipogenesis and may affect the mitochondrial function of mature adipocytes independent of differentiation, while inhibition of endogenous ceramide synthesis augments mitochondrial function in differentiating brown adipogenic progenitor cells. This corroborates the

previous observation that tissue-specific ablation of ceramide synthases in murine BAT or liver leads to an increase in energy expenditure and insulin sensitivity by enhancing thermogenesis in BAT [54]. Consistent with these observations, it was also reported that pharmacological inhibition of ceramide synthase stimulates browning of iWAT and increases insulin sensitivity, indicating that high synthesis rates of ceramides may indeed impair metabolic health of adipose tissues [55].

The signaling molecule sphingosine 1-phosphate (S1P), which is linked to ceramides as part of a biological rheostat, is often characterized as the counterpart of ceramides [39]. Somewhat contradictory, our data indicate a negative effect of S1P on the expression of brown adipogenic genes, whereas inhibition of S1P-signaling through its type 2 receptor, S1PR2, has the opposite effect. Reiterating this potential negative role of S1P in metabolic processes, it was reported that S1P concentrations in adipose tissue of obese subjects are increased [56]. Another study also showed that metabolic health and heat production were inversely correlated with circulating S1P levels. However, administration of S1P did not influence thermogenesis in this study, and neither was an agonist of S1PR1 effective, which is consistent with our own observations on this receptor, while S1PR2 was not tested [57].

The stimulatory effect of S1PR2-inhibition occurs independently of adrenergic stimulation, but has no additive effect when cells were co-stimulated with a β -agonist. Since both receptors are G-protein coupled, and β 3AR is coupled to a stimulatory G-protein, it stands to reason that S1PR2 may be coupled to a G-protein that counteracts the adrenergic signaling cascade. While the coupling of S1PR2 in brown adipocytes is unclear, it is known to couple to different types of G-proteins, including G_i and G_q [58]. G_q is a known negative regulator of brown adipocyte thermogenesis [59]. The negative effect of G_i on brown adipocytes has also been proposed before, and cold exposure has been shown to decrease G_i expression in BAT [60]. More importantly, an age-related increase of inhibitory G-proteins has been reported in adipocytes of aged rats [61]. In summary, these findings suggest that aging may result in altered concentrations of different sphingolipid species, including ceramides and S1P, which may attenuate brown adipocyte formation and their metabolic function.

Dolichols are established biomarkers of aging in different rodent and human tissues [62,63]. These isoprenoid chain-containing lipids are synthesized through the mevalonate pathway, which gives rise to important lipid mediators such as sterols and ubiquinones. Dolichols are alpha-saturated polyisoprenoids with a backbone of 14–24 isoprene subunits spanning all mammalian membranes. In the endoplasmic reticulum membrane, dolichols are the anchors for oligosaccharide synthesis for subsequent asparagine-linked N-glycosylation [64]. Our data show a strong accumulation of dolichols with variable isoprenoid chain lengths in BAT and iWAT of aged mice. Interestingly, it was shown that PC and PE, two lipid species upregulated by aging in BAT, activate dolichol kinase (*Dolk*), an enzyme which is highly expressed in BAT and phosphorylates dolichols to form bioactive lipids [37]. In our study, expression levels of *Dolk* were induced during aging and, in gain- and loss-of-function models, inversely correlated with thermogenic gene expression in brown adipocytes and may therefore participate in the age-related inhibition of BAT function. An upregulation of the enzymatic activity of *Dolk* may lead to different defects, including a more generalized endoplasmic reticulum stress due to attenuation of N-glycosylation and maturation of proteins, which requires further investigation.

5. CONCLUSION

The impairment of brown adipogenesis and mature brown adipocyte function may exacerbate metabolic diseases during aging and could at least in part be due to changed levels of different bioactive lipid species. The identification of biomarkers of BAT-aging, including regulatory metabolites that directly affect brown adipocyte formation and thermogenesis is necessary to understand the underlying molecular mechanisms of BAT regulation. We identify several lipid metabolites that are important regulators of brown adipocyte gene expression and therefore may serve as pharmaceutical targets to counter the age-related onset of obesity and metabolic complications.

AUTHOR CONTRIBUTIONS

T.J.S and S.G. conceived experiments, analyzed the majority of the data, and wrote the manuscript. S.G. performed the majority of experiments. A.C.I, V.Z., and M.M. performed lipidomic analyses and analyzed data. A.W., L.J., F.S., D.K., A.G., C.M., and H.S. performed experiments and helped analyze data. M.J. performed bioinformatics analyses. E.K., A.S., K.-J.P., and B.K. provided valuable resources and helped design some of the experiments.

ACKNOWLEDGMENTS

This work was supported by the German Research Foundation (DFG; grants SCHU 2445/2-1 and SCHU 2445/5-1, to T.J.S.), the European Research Council (ERC-StG 311082, to T.J.S.), the Paul Ehrlich Foundation (to T.J.S.) and a grant from the German Ministry of Education and Research (BMBF) and the State of Brandenburg (DZD grant 82DZD00302 and FKZ 82DZD0038G). This work was supported by NutriAct – Competence Cluster Nutrition Research Berlin-Potsdam funded by the Federal Ministry of Education and Research (FKZ: 01EA1408A-G) to B.K. Technical assistance by Nicole Dittberner, Antje Kretschmer, and Susann Richter is gratefully acknowledged.

CONFLICT OF INTEREST

None declared.

APPENDIX A. SUPPLEMENTARY DATA

Supplementary data to this article can be found online at <https://doi.org/10.1016/j.molmet.2019.03.011>.

REFERENCES

- [1] Cannon, B., Nedergaard, J., 2001. Respiratory and thermogenic capacities of cells and mitochondria from brown and white adipose tissue. *Methods in Molecular Biology* 155:295–303. <https://doi.org/10.1385/1-59259-231-7:295>.
- [2] Richard, D., Picard, F., 2011. Brown fat biology and thermogenesis. *Frontiers in Bioscience (Landmark Edition)* 16:1233–1260.
- [3] Cypess, A.M., Lehman, S., Williams, G., Tal, I., Rodman, D., Goldfine, A.B., et al., 2009. Identification and importance of brown adipose tissue in adult humans. *New England Journal of Medicine* 360:1509–1517. <https://doi.org/10.1056/NEJMoa0810780>.
- [4] Nedergaard, J., Bengtsson, T., Cannon, B., 2007. Unexpected evidence for active brown adipose tissue in adult humans. *American Journal of Physiology Endocrinology and Metabolism* 293:E444–E452. <https://doi.org/10.1152/ajpendo.00691.2006>.
- [5] Saito, M., Okamatsu-Ogura, Y., Matsushita, M., Watanabe, K., Yoneshiro, T., Nio-Kobayashi, J., et al., 2009. High incidence of metabolically active brown adipose tissue in healthy adult humans: effects of cold exposure and adiposity. *Diabetes* 58:1526–1531. <https://doi.org/10.2337/db09-0530>.
- [6] Himms-Hagen, J., Melnyk, A., Zingaretti, M.C., Ceresi, E., Barbatelli, G., Cinti, S., 2000. Multilocular fat cells in WAT of CL-316243-treated rats derive directly from white adipocytes. *American Journal of Physiology - Cell Physiology* 279:C670–C681.
- [7] Petrovic, N., Walden, T.B., Shabalina, I.G., Timmons, J.A., Cannon, B., Nedergaard, J., 2010. Chronic peroxisome proliferator-activated receptor gamma (PPARgamma) activation of epididymally derived white adipocyte cultures reveals a population of thermogenically competent, UCP1-containing adipocytes molecularly distinct from classic brown adipocytes. *Journal of Biological Chemistry* 285:7153–7164. <https://doi.org/10.1074/jbc.M109.053942>.
- [8] McDonald, R.B., Horwitz, B.A., 1999. Brown adipose tissue thermogenesis during aging and senescence. *Journal of Bioenergetics and Biomembranes* 31:507–516.
- [9] Florez-Duquet, M., Horwitz, B.A., McDonald, R.B., 1998. Cellular proliferation and UCP content in brown adipose tissue of cold-exposed aging Fischer 344 rats. *American Journal of Physiology* 274:R196–R203.
- [10] Florez-Duquet, M., McDonald, R.B., 1998. Cold-induced thermoregulation and biological aging. *Physiological Reviews* 78:339–358.
- [11] Avramoglu, R.K., Basciano, H., Adeli, K., 2006. Lipid and lipoprotein dysregulation in insulin resistant states. *Clinica Chimica Acta* 368:1–19. <https://doi.org/10.1016/j.cca.2005.12.026>.
- [12] Maurer, S.F., Dieckmann, S., Kleigrew, K., Colson, C., Amri, E.Z., Klingenspor, M., 2018. Fatty acid metabolites as novel regulators of non-shivering thermogenesis. *Handbook of Experimental Pharmacology*. https://doi.org/10.1007/164_2018_150.
- [13] Lynes, M.D., Shamsi, F., Sustarsic, E.G., Leiria, L.O., Wang, C.H., Su, S.C., et al., 2018. Cold-activated lipid dynamics in adipose tissue highlights a role for cardiolipin in thermogenic metabolism. *Cell Reports* 24:781–790. <https://doi.org/10.1016/j.celrep.2018.06.073>.
- [14] Sustarsic, E.G., Ma, T., Lynes, M.D., Larsen, M., Karavaeva, I., Havelund, J.F., et al., 2018. Cardiolipin synthesis in Brown and beige fat mitochondria is essential for systemic energy homeostasis. *Cell Metabolism* 28:159–174. <https://doi.org/10.1016/j.cmet.2018.05.003> e11.
- [15] Lynes, M.D., Leiria, L.O., Lundh, M., Bartelt, A., Shamsi, F., Huang, T.L., et al., 2017. The cold-induced lipokine 12,13-diHOME promotes fatty acid transport into brown adipose tissue. *Nature Medicine* 23:631–637. <https://doi.org/10.1038/nm.4297>.
- [16] Shi, H., Kokoeva, M.V., Inouye, K., Tzameli, I., Yin, H., Flier, J.S., 2006. TLR4 links innate immunity and fatty acid-induced insulin resistance. *Journal of Clinical Investigation* 116:3015–3025. <https://doi.org/10.1172/JCI28898>.
- [17] Blachnio-Zabielska, A.U., Hady, H.R., Markowski, A.R., Kurianiuk, A., Karwowska, A., Gorski, J., et al., 2018. Inhibition of ceramide de Novo synthesis affects adipocytokine secretion and improves systemic and adipose tissue insulin sensitivity. *International Journal of Molecular Sciences* 19. <https://doi.org/10.3390/ijms19123995>.
- [18] Szendroedi, J., Yoshimura, T., Phielix, E., Koliaki, C., Marcucci, M., Zhang, D., et al., 2014. Role of diacylglycerol activation of PKCtheta in lipid-induced muscle insulin resistance in humans. *Proceedings of the National Academy of Sciences of the United States of America* 111:9597–9602. <https://doi.org/10.1073/pnas.1409229111>.
- [19] Summers, S.A., Nelson, D.H., 2005. A role for sphingolipids in producing the common features of type 2 diabetes, metabolic syndrome X, and Cushing's syndrome. *Diabetes* 54:591–602.
- [20] Holland, W.L., Brozinick, J.T., Wang, L.P., Hawkins, E.D., Sargent, K.M., Liu, Y., et al., 2007. Inhibition of ceramide synthesis ameliorates glucocorticoid-, saturated-fat-, and obesity-induced insulin resistance. *Cell Metabolism* 5:167–179. <https://doi.org/10.1016/j.cmet.2007.01.002>.

- [21] Schulz, T.J., Huang, T.L., Tran, T.T., Zhang, H., Townsend, K.L., Shadrach, J.L., et al., 2011. Identification of inducible brown adipocyte progenitors residing in skeletal muscle and white fat. *Proceedings of the National Academy of Sciences of the United States of America* 108:143–148. <https://doi.org/10.1073/pnas.1010929108>.
- [22] Steinbring, J., Graja, A., Jank, A.M., Schulz, T.J., 2017. Flow cytometric isolation and differentiation of adipogenic progenitor cells into Brown and brite/beige adipocytes. *Methods in Molecular Biology* 1566:25–36. https://doi.org/10.1007/978-1-4939-6820-6_4.
- [23] Tseng, Y.H., Butte, A.J., Kokkotou, E., Yechoor, V.K., Taniguchi, C.M., Kriauciunas, K.M., et al., 2005. Prediction of preadipocyte differentiation by gene expression reveals role of insulin receptor substrates and neclin. *Nature Cell Biology* 7:601–611. <https://doi.org/10.1038/ncb1259>.
- [24] Kachler, K., Bailer, M., Heim, L., Schumacher, F., Reichel, M., Holzinger, C.D., et al., 2017. Enhanced acid sphingomyelinase activity drives immune evasion and tumor growth in non-small cell lung carcinoma. *Cancer Research* 77:5963–5976. <https://doi.org/10.1158/0008-5472.CAN-16-3313>.
- [25] Baylín, A., Kim, M.K., Donovan-Palmer, A., Siles, X., Dougherty, L., Tocco, P., et al., 2005. Fasting whole blood as a biomarker of essential fatty acid intake in epidemiologic studies: comparison with adipose tissue and plasma. *American Journal of Epidemiology* 162:373–381. <https://doi.org/10.1093/aje/kwi213>.
- [26] Metges, C.C., Lehmann, L., Boeuf, S., Petzke, K.J., Müller, A., Rickert, R., et al., 2003. cis-9,trans-11 and trans-10,cis-12 CLA affect lipid metabolism differently in primary white and brown adipocytes of Djungarian hamsters. *Lipids* 38:1133–1142.
- [27] Lange, S., Sylvester, M., Schumann, M., Freund, C., Krause, E., 2010. Identification of phosphorylation-dependent interaction partners of the adapter protein ADAP using quantitative mass spectrometry: SILAC vs (18)O-labeling. *Journal of Proteome Research* 9:4113–4122. <https://doi.org/10.1021/pr1003054>.
- [28] Chen, E.Y., Tan, C.M., Kou, Y., Duan, Q., Wang, Z., Meirelles, G.V., et al., 2013. Enrichr: interactive and collaborative HTML5 gene list enrichment analysis tool. *BMC Bioinformatics* 14:128. <https://doi.org/10.1186/1471-2105-14-128>.
- [29] Kuleshov, M.V., Jones, M.R., Rouillard, A.D., Fernandez, N.F., Duan, Q., Wang, Z., et al., 2016. Enrichr: a comprehensive gene set enrichment analysis web server 2016 update. *Nucleic Acids Research* 44:W90–W97. <https://doi.org/10.1093/nar/gkw377>.
- [30] Huang, D.W., Sherman, B.T., Lempicki, R.A., 2009. Systematic and integrative analysis of large gene lists using DAVID bioinformatics resources. *Nature Protocols* 4:44–57. <https://doi.org/10.1038/nprot.2008.211>.
- [31] Supek, F., Bosnjak, M., Skunca, N., Smuc, T., 2011. REVIGO summarizes and visualizes long lists of gene ontology terms. *PLoS One* 6:e21800. <https://doi.org/10.1371/journal.pone.0021800>.
- [32] Giavalisco, P., Kohl, K., Hummel, J., Seiwert, B., Willmitzer, L., 2009. 13C isotope-labeled metabolomes allowing for improved compound annotation and relative quantification in liquid chromatography-mass spectrometry-based metabolomic research. *Analytical Chemistry* 81:6546–6551. <https://doi.org/10.1021/ac900979e>.
- [33] Fiehn Laboratory, 2016. UC DAVIS. <http://fiehnlab.ucdavis.edu/>.
- [34] Smith, C.A., O'Maille, G., Want, E.J., Qin, C., Trauger, S.A., Brandon, T.R., et al., 2005. METLIN: a metabolite mass spectral database. *Therapeutic Drug Monitoring* 27:747–751.
- [35] Sud, M., Fahy, E., Cotter, D., Brown, A., Dennis, E.A., Glass, C.K., et al., 2007. LMSD: LIPID MAPS structure database. *Nucleic Acids Research* 35:D527–D532. <https://doi.org/10.1093/nar/gkl838>.
- [36] Metsalu, T., Vilo, J., 2015. ClustVis: a web tool for visualizing clustering of multivariate data using Principal Component Analysis and heatmap. *Nucleic Acids Research* 43:W566–W570. <https://doi.org/10.1093/nar/gkv468>.
- [37] Genain, C.P., Waechter, C.J., 1990. Separation of brain dolichol kinase from endogenous activating factors: evidence that phospholipid enhances the interaction between enzyme and dolichol. *Journal of Neurochemistry* 54:855–862.
- [38] Parentini, I., Cavallini, G., Donati, A., Gori, Z., Bergamini, E., 2005. Accumulation of dolichol in older tissues satisfies the proposed criteria to be qualified a biomarker of aging. *Journals of Gerontology Series A: Biological and Medical Sciences* 60:39–43.
- [39] Spiegel, S., Milstien, S., 2003. Sphingosine-1-phosphate: an enigmatic signalling lipid. *Nature Reviews Molecular Cell Biology* 4:397–407. <https://doi.org/10.1038/nrm1103>.
- [40] Keller, R.K., 1996. Squalene synthase inhibition alters metabolism of non-sterols in rat liver. *Biochimica et Biophysica Acta* 1303:169–179.
- [41] BioGPS, 2018. <http://ds.biogps.org/?dataset=GSE10246&gene=227697>.
- [42] Rogers, N.H., Landa, A., Park, S., Smith, R.G., 2012. Aging leads to a programmed loss of brown adipocytes in murine subcutaneous white adipose tissue. *Aging Cell* 11:1074–1083. <https://doi.org/10.1111/acer.12010>.
- [43] Kirkland, J.L., Dax, E.M., 1984. Adipocyte hormone responsiveness and aging in the rat: problems in the interpretation of aging research. *Journal of the American Geriatrics Society* 32:219–228.
- [44] Steculorum, S.M., Ruud, J., Karakasilioti, I., Backes, H., Engstrom Ruud, L., Timper, K., et al., 2016. AgRP neurons control systemic insulin sensitivity via myostatin expression in Brown adipose tissue. *Cell* 165:125–138. <https://doi.org/10.1016/j.cell.2016.02.044>.
- [45] Brown, A.J., Goldsworthy, S.M., Barnes, A.A., Eilert, M.M., Tcheang, L., Daniels, D., et al., 2003. The Orphan G protein-coupled receptors GPR41 and GPR43 are activated by propionate and other short chain carboxylic acids. *Journal of Biological Chemistry* 278:11312–11319. <https://doi.org/10.1074/jbc.M211609200>.
- [46] Aberdein, N., Schweizer, M., Ball, D., 2014. Sodium acetate decreases phosphorylation of hormone sensitive lipase in isoproterenol-stimulated 3T3-L1 mature adipocytes. *Adipocyte* 3:121–125. <https://doi.org/10.4161/adip.27936>.
- [47] den Besten, G., van Eunen, K., Groen, A.K., Venema, K., Reijngoud, D.J., Bakker, B.M., 2013. The role of short-chain fatty acids in the interplay between diet, gut microbiota, and host energy metabolism. *The Journal of Lipid Research* 54:2325–2340. <https://doi.org/10.1194/jlr.R036012>.
- [48] Bjursell, M., Admyre, T., Goransson, M., Marley, A.E., Smith, D.M., Oscarsson, J., et al., 2011. Improved glucose control and reduced body fat mass in free fatty acid receptor 2-deficient mice fed a high-fat diet. *American Journal of Physiology. Endocrinology and Metabolism* 300:E211–E220. <https://doi.org/10.1152/ajpendo.00229.2010>.
- [49] Fajardo, V.A., McMeekin, L., LeBlanc, P.J., 2011. Influence of phospholipid species on membrane fluidity: a meta-analysis for a novel phospholipid fluidity index. *Journal of Membrane Biology* 244:97–103. <https://doi.org/10.1007/s00232-011-9401-7>.
- [50] Bonzon-Kulichenko, E., Molto, E., Pintado, C., Fernandez, A., Arribas, C., Schwudke, D., et al., 2018. Changes in visceral adipose tissue plasma membrane lipid composition in old rats are associated with adipocyte hypertrophy with aging. *Journals of Gerontology Series A: Biological and Medical Sciences* 73:1139–1146. <https://doi.org/10.1093/gerona/gly081>.
- [51] Niemela, P.S., Ollila, S., Hyvonen, M.T., Karttunen, M., Vattulainen, I., 2007. Assessing the nature of lipid raft membranes. *PLoS Computational Biology* 3:e34. <https://doi.org/10.1371/journal.pcbi.0030034>.
- [52] Paradies, G., Ruggiero, F.M., Gadaleta, M.N., Quagliariello, E., 1992. The effect of aging and acetyl-L-carnitine on the activity of the phosphate carrier and on the phospholipid composition in rat heart mitochondria. *Biochimica et Biophysica Acta* 1103:324–326.
- [53] Simopoulos, A.P., 2016. An increase in the omega-6/omega-3 fatty acid ratio increases the risk for obesity. *Nutrients* 8:128. <https://doi.org/10.3390/nu8030128>.
- [54] Turpin, S.M., Nicholls, H.T., Willmes, D.M., Mourier, A., Brodessa, S., Wunderlich, C.M., et al., 2014. Obesity-induced CerS6-dependent C16:

- 0 ceramide production promotes weight gain and glucose intolerance. *Cell Metabolism* 20:678–686. <https://doi.org/10.1016/j.cmet.2014.08.002>.
- [55] Chaurasia, B., Kaddai, V.A., Lancaster, G.I., Henstridge, D.C., Sriram, S., Galam, D.L., et al., 2016. Adipocyte ceramides regulate subcutaneous adipose browning, inflammation, and metabolism. *Cell Metabolism* 24:820–834. <https://doi.org/10.1016/j.cmet.2016.10.002>.
- [56] Ito, S., Iwaki, S., Koike, K., Yuda, Y., Nagasaki, A., Ohkawa, R., et al., 2013. Increased plasma sphingosine-1-phosphate in obese individuals and its capacity to increase the expression of plasminogen activator inhibitor-1 in adipocytes. *Coronary Artery Disease* 24:642–650. <https://doi.org/10.1097/MCA.0000000000000033>.
- [57] Green, C.L., Mitchell, S.E., Deros, D., Wang, Y., Chen, L., Han, J.J., et al., 2017. The effects of graded levels of calorie restriction: IX. Global metabolomic screen reveals modulation of carnitines, sphingolipids and bile acids in the liver of C57BL/6 mice. *Aging Cell* 16:529–540. <https://doi.org/10.1111/ace.12570>.
- [58] Chen, W., Lu, H., Yang, J., Xiang, H., Peng, H., 2016. Sphingosine 1-phosphate in metabolic syndrome (Review). *International Journal of Molecular Medicine* 38:1030–1038. <https://doi.org/10.3892/ijmm.2016.2731>.
- [59] Klepac, K., Kilic, A., Gnad, T., Brown, L.M., Herrmann, B., Wilderman, A., et al., 2016. The Gq signalling pathway inhibits brown and beige adipose tissue. *Nature Communications* 7:10895. <https://doi.org/10.1038/ncomms10895>.
- [60] Svoboda, P., Unelius, L., Dicker, A., Cannon, B., Milligan, G., Nedergaard, J., 1996. Cold-induced reduction in Gi alpha proteins in brown adipose tissue. Effects on the cellular hypersensitization to noradrenaline caused by pertussis-toxin treatment. *Biochemical Journal* 314(Pt 3):761–768.
- [61] Green, A., Gasic, S., Milligan, G., Dobias, S.B., 1995. Increased concentrations of proteins Gi1 and Gi2 in adipocytes from aged rats alter the sensitivity of adenylyl cyclase to inhibitory and stimulatory agonists. *Metabolism* 44:239–244.
- [62] Daniels, I., Hemming, F.W., 1990. Changes in murine tissue concentrations of dolichol and dolichol derivatives associated with age. *Lipids* 25:586–593.
- [63] Kalen, A., Appelkvist, E.L., Dallner, G., 1989. Age-related changes in the lipid compositions of rat and human tissues. *Lipids* 24:579–584.
- [64] Burda, P., Aebi, M., 1999. The dolichol pathway of N-linked glycosylation. *Biochimica et Biophysica Acta* 1426:239–257.